Use of Nanostructures for High Brightness Light-Emitting Diodes

G. B. Stringfellow

Abstract Light-emitting diodes or LEDs are expected to play a major role in efforts to utilize less energy for lighting applications due to their high efficiency, long operating life, and other "green" characteristics. The history of LEDs began in the 1960s. Since that time, the performance has increased exponentially while the cost has decreased dramatically. LEDs dominate the market for monochromatic displays and indicators, and are slated to provide an increasing share of the white light market. During the last decade, advances in efficiency have been obtained partly as a result of the use of nanotechnology. LEDs and lasers provided some of the first applications for quantum-well structures with nm dimensions. Future advances will almost certainly be linked to advances in the use of quantum wire and quantum dot structures. They appear to offer attractive new alternatives for single-junction white light generation. The use of self-assembled structures also offers the promise of allowing the fabrication of high efficiency devices in highly defected materials, such as those grown on less expensive substrates. This chapter reviews the basic aspects of LED devices and materials, with a focus on the AlGaInP system for red and yellow emitters and AlGaInN for blue, green, and white emitters, all grown by the organometallic vapor phase epitaxial technique. The focus is on the present and future use of nanotechnology for lighting applications.

G. B. Stringfellow (✉)
Department of Materials Science and Engineering, University of Utah,
Salt Lake City, UT, USA
e-mail: stringfellow@eng.utah.edu

L. Zang (ed.), *Energy Efficiency and Renewable Energy Through Nanotechnology*,
Green Energy and Technology, DOI: 10.1007/978-0-85729-638-2_23,

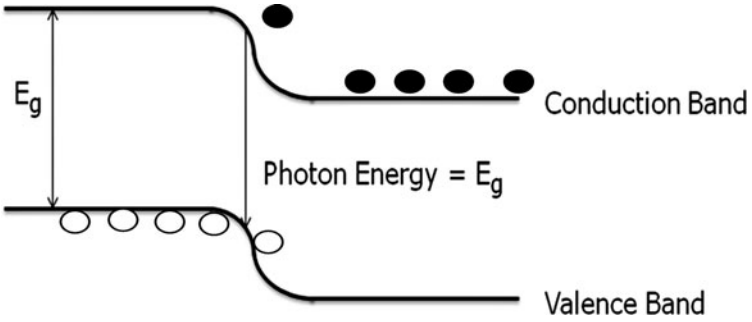

Fig. 1 Schematic diagram of a LED structure showing the electron–hole recombination giving a photon with energy equal to the bandgap energy

1 Introduction

Light emitting diodes, or LEDs, are p/n junction semiconductor devices that convert electrons flowing through the device into nearly monochromatic photons, as shown schematically in Fig. 1, with an energy (color) determined by the bandgap energy of the semiconductor. Using two III/V alloy systems, AlInGaP and AlInGaN, the bandgaps can be tuned to give highly efficient generation of any color of the visible spectrum, as well as IR or UV light, as shown in Figs. 2 and 3. LEDs have much longer operating lifetimes than any other conventional light source. They can operate continuously for as long as 10 years (100,000 h) before the light output declines significantly and normally do not fail catastrophically. Because the LEDs are typically small, about the size of a grain of salt, the direction of light output is easily tailored to suit particular applications. They turn on and off in less than a microsecond, so there is no irritating delay, as for fluorescent lights, and they can be used with dimmers. Their rapid modulation capability also allows the use of LEDs and lasers in high-bandwidth, optical communications applications. Furthermore, LEDs do not contain harmful substances, such as mercury, so they are much more environmental friendly.

Light emitting diodes are sometimes referred to as the "ultimate light bulb" because they approach the theoretical maximum efficiency for turning electrical current into light. External quantum efficiencies (photons out per electron in) exceeding 50% have been achieved in both the red and blue regions of the spectrum. The efficiency is plotted as a function of photon wavelength in Fig. 4 [36–38, 51, 57, 58, 95]. It is seen that the efficiency is not as high in the mid-spectral range, resulting in the so-called "green gap".

LEDs are inherently monochromatic; thus, they are more than 20 times more efficient than filtered incandescent lights for applications requiring a particular color, such as the red brake lights on cars and the red, green, and amber lights in traffic semaphores. This, plus their very long operating lives, has led to their complete dominance for these applications. Even for white lights, LEDs are more efficient by over a factor of five compared to incandescent sources. They are

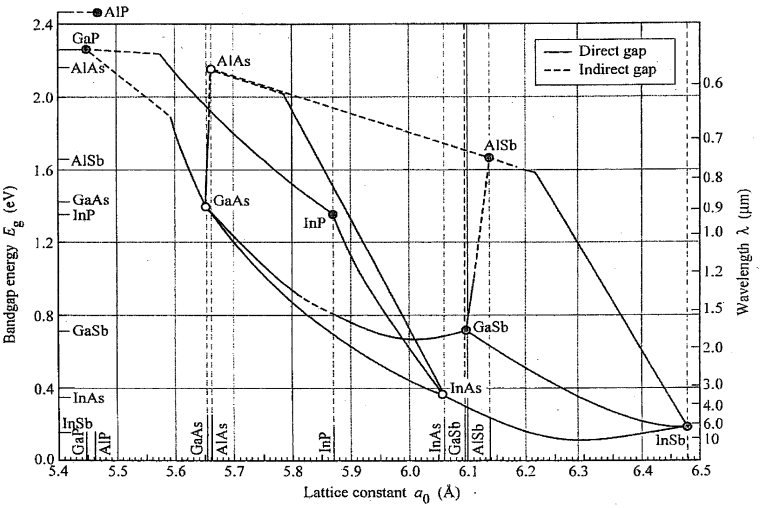

Fig. 2 Energy gap vs lattice constant for common semiconductor elements, compounds, and alloys not containing nitrogen (after P. K. Tien, 1988, Unpublished work from AT&T Bell Laboratories with permission)

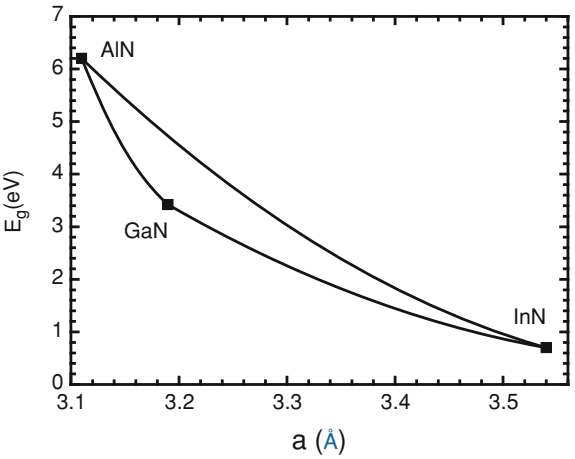

Fig. 3 Bandgap versus lattice constant for AlInGaN alloys (after Stringfellow [85], with permission)

significantly more expensive than conventional light bulbs, but their efficiency and long operating life make them economically preferable to conventional light bulbs after less than 2 years of operation. Since 50% of residential lighting is provided by 60 Watt incandescent bulbs, replacement by white LED light bulbs offers a potentially staggering savings in energy usage. If all incandescent lamps in the USA were replaced by LEDs, the energy savings would be approximately 1000 TW-h/year (estimated to be equivalent to the energy used to light 15 million homes), representing cost savings of $100 B/year. This would also lead to a decrease in the annual amount of carbon emissions into the atmosphere of 200 M

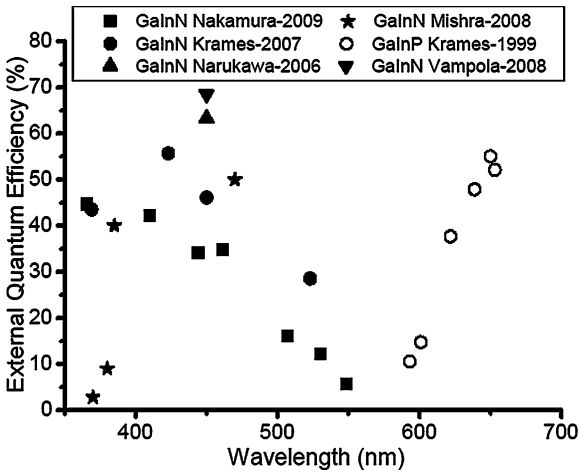

Fig. 4 External quantum efficiency of LEDs versus emission wavelength comparing data for AlInGaN (solid data points) with AlInGaP (open data points)

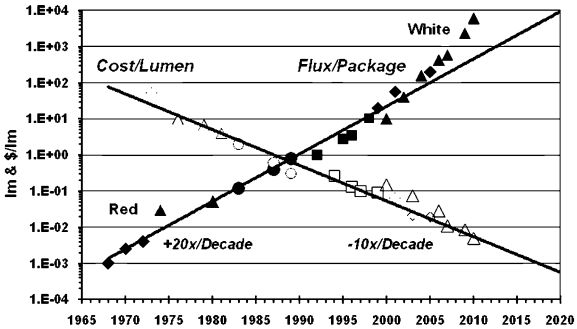

Fig. 5 Time evolution of LED luminous flux and purchase price per lumen (R. Haitz, 2010, private communication)

tons [38]. In the near future, the efficiencies of white lights will increase somewhat and the cost will decrease dramatically, as is common with virtually all semiconductor devices; as the volume increases the unit cost decreases. Both trends are shown in Fig. 5 (Haitz 2010). The sales volume of white LED lights has soared recently due to applications where LEDs dominate on the basis of factors other than cost, such as headlamps for automobiles and the light sources for backlit liquid–crystal display (LCD) television screens. The competing plasma TV screens are so energy inefficient that they have been banned in California after 2011. It is estimated that the switch to LCD/LED TVs will save $8.1 billion in energy costs according to the California Energy Commission, as reported by NewsFactor on November 20, 2009.

The other light-emitting device that will be discussed in this chapter is the injection laser. It operates on the same principle as the conventional LED. In fact, the laser operates as an LED until a certain threshold current is exceeded. For higher currents, stimulated emission dominates spontaneous emission and the

device emits a high-intensity laser beam. For a laser, the p/n junction is enclosed in an optical cavity to allow a build-up of photon intensity to promote stimulated emission.

Lasers in the visible region of the spectrum are used in display and projection applications. They are also the key components of optical memories, including CD and DVD drives. Lasers are necessary components of high speed optical communication systems. The optimum wavelengths for high frequency, long-distance communications is in the IR, at either 1.3 or 1.55 μm. These lasers are typically fabricated in the InGaAsP quaternary alloy system [34, 83, Chap. 10]. Operation in the red region of the spectrum is suitable for short distance communication via plastic fibers. Si detectors have their maximum photon detection efficiency in the red. Red semiconductor lasers are also being considered for quantum cryptography applications, where single photon sources are required [72]. A particularly important application is for high speed optical interchip communications. This requires integration of III/V lasers with the Si ICs. Thus, the growth of high quality III/V semiconductors on Si is an area of intense research activity.

The performance of LEDs has evolved exponentially over the last 30 years with order-of-magnitude increases in efficiency coupled with order-of-magnitude decreases in cost, as seen in Fig. 5. The threshold current densities of lasers have decreased by orders of magnitude during this time. These advances have been based on an increased understanding and control of the materials properties as well as the device and package design. The importance of the formation and control of nanostructures has played a central role in these advances. Future efforts to reach higher performance at lower device costs appear to be dependent on developing techniques for the low-cost use of other nanostructures, including quantum wells, quantum wires, and quantum dots (QDs), nanostructures with reduced dimensionality in 1–3 dimensions, respectively.

Some benefits of nanostructures for laser performance are similar to those seen for LEDs; however, there are certain aspects of laser devices where the use of nanostructures is even more important. For example, the use of low-dimensional structures produces a density of states that is optimal for low threshold current densities [100, p. 213], as discussed in Sect. 4. In addition, the temperature dependence of the threshold current density is much superior for lasers fabricated in low-dimensional structures. The temperature dependence completely disappears for ideal QD lasers [100, p. 212]. The large band offsets in InP/AlInGaP QD structures is considered to be important for the fabrication of red-emitting lasers for quantum information applications [72]. In addition, the use of quantum wire structures to mitigate lattice-mismatch effects is a promising approach to the fabrication of high-performance lasers on Si for optical interconnect applications [92]. Finally, the concept of self-assembled laser structures in nanowires offers tremendous promise [3], especially since, in some ways, the performance of nanowire structures is superior to typical quantum-well device structures.

State-of-the-art LED and laser materials, structures, and devices are complex. Since all commercial LEDs and lasers are composed of III/V semiconductors and their alloys, this chapter will be limited to a discussion of these materials.

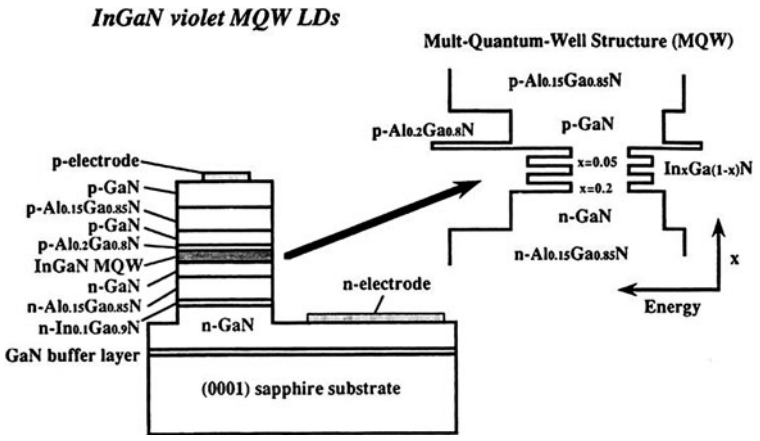

Fig. 6 The structure of InGaN MQW laser diode (after Nakamura [56], with permission)

An overview of the materials used can be obtained by examining the plots of bandgap energy versus lattice constant, Figs. 2 and 3. The bandgap energy is depicted as a unique function of solid composition in these plots, which is true only for random alloys. In other words, the effects of micro-and nano-structure have been neglected. This will be rectified in later sections. The two main materials for LEDs are the AlInGaP system, for red, orange, and yellow LEDs, and the AlInGaN system, for blue, green, and white LEDs. These two materials will be the focus of this chapter.

A high-performance LED or laser typically consists of several tens of layers of different semiconductor materials grown epitaxially on a particular substrate, as illustrated in Fig. 6. In order to emit light efficiently, the semiconductor materials must be direct bandgap and single crystalline, having a low density of mechanical defects, such as dislocations, and point defects including impurities, vacancies, interstitials, etc. This means that the materials and structures used in LED and laser devices must be grown by epitaxial techniques on single-crystalline substrates. Several epitaxial techniques have been used. Liquid phase epitaxy (LPE) and hydride vapor phase epitaxy (HVPE) were used for early LED and laser devices, but in the last two decades molecular beam epitaxy (MBE) and, particularly, organometallic vapor phase epitaxy (OMVPE—sometimes written MOVPE or MOCVD) have become predominant.

For the wavelengths required for specific applications, the simultaneous achievement of both increasing performance (efficiency of converting electrons into photons escaping from the device) and lower cost represents the basic challenge of LEDs and lasers in the coming decade. Reductions in cost are often obtained at the expense of creating more defects. One way of producing efficient light production in defected materials is to localize the recombination of electrons and holes to produce photons in small regions of highly perfect material using nanostructures, as discussed in Sect. 4.

Before examining the details of the semiconductor materials and structures used in light-emitting devices, with an emphasis on the role of nanostructures, it is worthwhile to enumerate the overarching concerns.

The first requirement is the ability to produce perfect and pure single-crystalline layers capable of high efficiency conversion of electrons crossing the p/n junction into photons of a particular wavelength (bandgap energy), determined by the application. Modern device structures require that multiple layers of several different materials be stacked upon one another via epitaxial growth.

A high conversion efficiency for the production of photons of a specified wavelength requires two factors: a high radiative recombination efficiency, or a short radiative lifetime, which, in turn, requires a direct bandgap and a large overlap of electron and hole wavefunctions and a long non-radiative lifetime, i.e., a slow rate of wasteful recombination that does not produce photons.

The ultimate goal is to have a high conversion efficiency even in a material with a high density of defects, such as dislocations. This would allow the growth of the desired layers on a substrate having a dissimilar lattice constant. Particularly important would be the growth of III/V structures on Si substrates. The ability to allow the various layers to have different lattice parameters is also highly desirable.

The photons produced at the p/n junction must be extracted efficiently, i.e., a large fraction must exit the device, rather than being absorbed.

The high conversion efficiency must be maintained at very high current densities while maintaining a long operating life. This allows for the efficient use of the expensive LED structures, i.e., more photons are extracted per unit area of the device. A problem observed for LEDs fabricated in the InGaN system is the so-called "droop", where the photon intensity becomes nearly constant (i.e., the efficiency decreases) for high current densities [38].

All of the above must be accomplished at a reasonable cost, since LED lighting competes directly with the very well-developed and low-cost alternatives of incandescent and fluorescent lighting.

In this introduction, these factors will be discussed briefly with special emphasis on the role of nanotechnology in producing the desired results. Later, in Sect. 4, the use of nanostructures will be described in more detail, followed by descriptions of the use of nanostructures to improve the performance of LEDs in several specific III/V materials systems.

This chapter will emphasize the use of single-crystalline III/V alloys for the production of visible photons. Organic LEDs are also used, especially for low-cost devices, but will not be discussed here. Other compound semiconductors can also be used for crystalline semiconductor LEDs, but all commercial LEDs are produced in III/V materials. Thus, this chapter will discuss only single-crystalline III/V semiconductor systems with emphasis on the two quaternary alloys AlInGaP and AlInGaN. The commercial production of LEDs in both of these materials systems uses the technique of OMVPE. This technique is versatile, so it can produce all of the materials and structures, including quantum wells, quantum wires, and QDs, required for LEDs and lasers. Thus, this chapter will focus on the

OMVPE technique, although results from layers grown by other techniques will be included where they add to our understanding of the effects of the nanostructure on materials properties and device performance.

The choice of bandgap energy nominally determines the color of the emitted light. Every color is needed between red (Eg = 1.9 eV) and blue (Eg = 2.5 eV) for various applications. This determines the materials from which the LEDs are fabricated, as indicated in Figs. 2 and 3. Devices emitting in the IR and UV spectral regions are also important for non-lighting applications.

The three primary colors, red, green, and blue, are required for white light and full color displays. The initial approach to making an LED of a particular color was based on the idea that the selection of solid composition uniquely determines the bandgap energy or the color of the light emitted from a particular material. For example, the lines shown in Figs. 2 and 3 are meant to indicate the bandgap energy of particular alloy compositions in the various bulk III–V materials (i.e., with no quantum confinement). However, more recently it has become clear that the solid composition does not uniquely determine the materials properties; the microstructure (more appropriately, the nanostructure) is a major determinant of the properties of alloy semiconductors and the devices made from them. The judicious control of nanostructure is an invaluable tool in the arsenal of modern materials and device designers. For example, the use of low-dimensional structures having dimensions smaller than the de Broglie wavelength of an electron, i.e., of dimensions of 1–30 nm, in 1, 2, or 3 directions allows tailoring of the emission energy (LED color) due to the quantum size effect. Confinement of electrons and holes together in these small regions can be used to improve the radiative recombination efficiency. Nanostructures can also have a positive effect on the light extraction efficiency as described in Sect. 4.1.

The use of quantum wells, where the electron and hole wave functions are confined in 1 direction, forming a two-dimensional (2D) system, was one of the first practical applications of nanotechnology for any material. A seminal paper by Dingle et al. [15] demonstrated that the bandgap of GaAs could be increased when a thin layer was sandwiched between higher bandgap AlGaAs layers, with the entire quantum-well structure grown by MBE. Today, quantum wells are used in essentially every commercial LED and laser device as a means of improving device performance. Subsequently, quantum wires and QDs, giving 1D and 0D systems, respectively, have been found to give additional enhancements in the performance of both LEDs and lasers as described in Sect. 4.1. The use of such nanostructures promises to improve green, and perhaps yellow and red, AlInGaN LEDs. The efficiency of green LEDs is much lower than for red and blue LEDs, as seen in Fig. 4. Nanostructures are being actively explored for the production of improved green laser and LED devices in the AlInGaN materials system. A particularly important example currently under intensive investigation is the use of QDs to allow the production of single-junction LEDs that the human eye perceives as white. Of course, white LEDs must emit at several wavelengths which, when added together, produce white light. This can be achieved by combining individual monochromatic LEDs of the three primary colors, red, green,

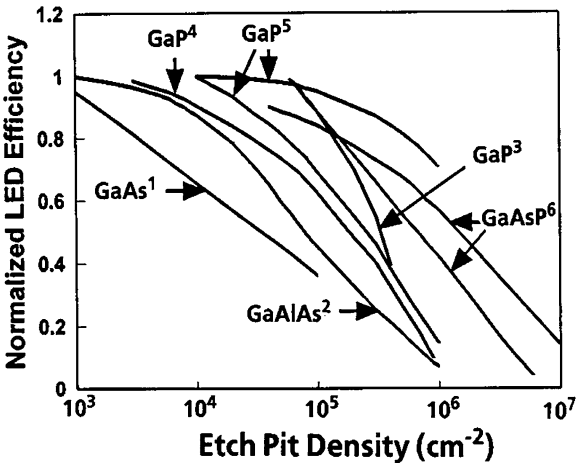

Fig. 7 LED efficiency versus dislocations density for conventional III/V materials (reprinted with permission from Lester et al. [47]. Copyright (1995), American Institute of Physics)

and blue (the RGB approach). In the future, the goal is to produce a single LED that simultaneously produces 2 or more colors that combine to produce light that appears white.

For the III/V semiconductors used in LEDs, the choice of the substrate material is vital. When the crystal structure and lattice constant of the epitaxial layer match those of the substrate, virtually perfect epitaxial layers can be produced. This severely limits the choice of materials for LEDs. As seen in Fig. 2, one choice for a so-called "lattice matched" system would be the growth of an InGaP epitaxial layer on a GaAs substrate; however, only one InGaP alloy satisfies this constraint, that with an InP mole fraction of approximately 0.5. When this condition is not satisfied, the lattice parameter mismatch gives rise to dislocations, generated to relieve the strain, which are formed in the interface plane and propagate up through the epitaxial layer. These dislocations have been known for decades to severely degrade device performance, as shown in Fig. 7 [47]. For high LED performance, dislocation densities of 10^4 cm^{-2} and less are needed for conventional III/V materials. The nitrides behave differently, which appears to be related to a spontaneously generated nanostructure, as discussed in detail in Sect. 4.3.

One approach to improve lattice-mismatched systems for LEDs is to develop a so-called "conformal" substrate. Such substrates allow the strain from the mismatch to be confined to the substrate, i.e., the substrate deforms to allow the growth of a dislocation-free epitaxial layer. All of the strain and any dislocations generated will be entirely confined to the substrate, where they will have no deleterious effect on device performance. This has been a topic of research for more than a decade, with less than satisfactory results for the large substrates required in order to contain the cost per device [9]. It will not be discussed further here, although there remains some hope of ultimate success.

A more promising approach is to form the light-emitting regions of the device in nano-wires or -rods that extend in a direction perpendicular to the

substrate. For these very thin, wire-shaped single-crystalline materials, a change in lattice constant is accommodated elastically, by lateral relaxation of the wire, without the generation of dislocations [8]. This approach offers promise for the production of III/V lasers on Si substrates for inter chip IC communications [92]. Elastic deformation of the wire allows structures with a change in lattice constant along the length of the wire to be grown without the generation of misfit dislocations. For the "core/shell" structure, where the change in lattice constant occurs in the lateral direction, the layers are strained, but dislocations are not generated.

Another approach that uses nanotechnology is to somehow "passivate" the misfit dislocations produced in the epitaxial layer, i.e., to allow the efficient generation of photons even in a material with a very high dislocation density. This idea was first suggested for GaAs grown on Si substrates [23, 99]. It is an area where nanotechnology is believed to play a vital role for LEDs fabricated in the AlInGaN system, as discussed in Sect. 4.

Finally, the photons produced at the p/n junction must be extracted efficiently in order to produce a high efficiency LED. More than a decade ago, techniques were developed to minimize the absorption of photons within the semiconductor material [35], which often involves the removal of the absorbing substrate and wafer bonding to a new transparent "substrate". Use of nanowire growth to remove the lattice-match constraint might allow this expensive step to be eliminated.

In addition, techniques have been developed to reduce the change in refractive index experienced by the photons as they exit the high refractive index LED materials. This may involve coating the LEDs with high index, transparent materials. Shaping of the individual diodes is also used to enhance light extraction [36]. More recently, the use of nanotechnology has been developed to produce surfaces structures to enhance the light extraction efficiency [28].

Important aspects of controlling the cost of LEDs include: increasing yield in large-scale production techniques giving excellent uniformity of thickness and solid composition for the multiple thin layers of which the LED is composed; decreasing the cost of the substrate by using inexpensive materials or by developing processes to allow the re-use of the substrate; and producing materials that emit light with high external efficiencies at very high current densities for very long times, which allows a minimum of material to be used for the LED. Of course, the cost of the LED will scale with the device area for a given optical output. Currently, the efficiency of light output of blue and green GaN LEDs begins to "droop" at high current densities. The cause has not been unambiguously identified, but the use of nanotechnology is being explored to solve the problem.

In the remainder of this chapter, we will first review the fundamental aspects of LED performance, including the benefits of using nanotechnology to improve both cost and performance, the generation of light at a p/n junction and the extraction of the photons from the device. This will be followed by a review of the OMVPE growth technique used for the production of LED materials and structures. Finally, this background will be used as the basis of a discussion of the practical application of nanotechnology for LEDs and lasers in several specific systems, with an

emphasis on LEDs emitting in the red-yellow spectral region, made from AlInGaP, and the green–blue spectral region, made from AlInGaN, including the use of this material for white LEDs.

2 LED Devices

The two major factors that must be optimized to produce an efficient LED are the recombination efficiency and the optical extraction efficiency. Both factors can be significantly enhanced via the judicious use of nanostructures.

Consider first the internal quantum efficiency, the fraction of electrons traversing the p/n junction that produce photons. The rate of the radiative process which produces the desired visible photons is the product of the np product and the recombination coefficient B_r [89, Chap. 13],

$$R_r = npB_r. \tag{1}$$

The former is determined by the majority carrier concentration and the deviation from equilibrium, i.e., the injected minority carrier concentration, and the latter by the fundamental properties of the semiconductor material, principally the band structure. Direct bandgap materials, where the conduction band minimum and the valence band maximum occur at the same place in k-space, allow rapid recombination of electrons and holes, with conservation of energy allowed by the creation of a photon with an energy equal to the difference in energy between the electron and hole in their initial states, as shown in Fig. 1. In indirect bandgap materials, a third particle, a phonon, is required to allow conservation of momentum. Because it is indirect, Si is a poor material for light emission. The high-bandgap energy III/V semiconductors may also be indirect, as shown in Fig. 2, where direct bandgap materials are indicated using solid lines and indirect materials by broken lines. Indirect bandgap materials can be used for LEDs [71, Chap. 12]; however, all commercial devices are made from direct materials. Thus, the LED and laser materials described in this chapter will be restricted to those with direct bandgaps.

At this point it is worth mentioning that when an indirect bandgap material is produced as low-bandgap QDs dispersed in a higher bandgap semiconductor, the bandgap may become direct [91], thus increasing the radiative recombination coefficient. In the simplest case, conservation of momentum becomes a simple selection rule, e.g., $\Delta n = 0$ [100, p. 65], where Δn is the difference in quantum numbers for the confined electron and hole states. However, in real systems, the converse, direct to indirect transitions, may occur for small QDs [49].

The electrons in the conduction band and holes in the valence band can also recombine non-radiatively. This normally occurs via defects either in the bulk (point defects or dislocations) or on the surface. Many III/V semiconductors have very high surface recombination rates. In general the non-radiative recombination rate is given by the equation [89, Chap. 13]:

$$R_{nr} = N_t \sigma v_{th} \Delta p, \tag{2}$$

where N_t is the concentration of defects, σ the capture cross-section, v_{th} the thermal velocity, and Δp the injected hole concentration, assuming the semiconductor to be n-type. The internal quantum efficiency is the ratio of the rate of radiative recombination to the total recombination rate, written

$$\eta_{int} = R_r/(R_r + R_{nr}). \tag{3}$$

High internal quantum efficiencies require both high values of B_r and low defect densities. Both of these factors can be enhanced in non-classical ways by using nanostructures. As the dimensionality of the recombination volume decreases, the electron and hole wavefunctions are forced to overlap, which increases the quantum mechanical matrix element for radiative recombination and, consequently, B_r. In addition, the exciton binding energy increases making excitonic recombination dominant, even at room temperature, which also increases the radiative recombination rate [100, p. 64].

An additional factor that affects B_r in (0001) quantum wells in the AlInGaN system is the quantum confined Stark effect (QCSE), which *decreases* the value of B_r. This is a serious issue for blue and green LEDs. One approach to circumventing this problem involves growing the quantum-well structures on crystallographic directions other than (0001), where the piezoelectric effect does not occur [57]. The use of very small QDs also appears to offer promise for reducing the QCSE by forcing an increase in wavefunction overlap, as discussed in Sect. 4.1 [54].

In addition to increasing the radiative recombination rate, nanostructures can also be used to suppress non-radiative recombination simply by insuring that the minority carriers are not able to diffuse to non-radiative defects [69, 85]. The diffusion of minority carriers can be reduced by producing fluctuations in the conduction and valence bands due to the controlled formation of compositional fluctuations. One way of producing spontaneous compositional fluctuations is to take advantage of the natural phenomenon of phase separation (PS) or spinodal decomposition [85]. This is generally believed to enhance the internal efficiency in InGaN LEDs. PS may also be a mechanism to explain the very high recombination efficiency observed in InGaN quantum wires, as compared with epitaxial layers [41], as discussed in Sect. 4.3. The effects of nanostructures on LED performance will be considered in more detail in Sect. 4.1.

The second major factor affecting LED performance is the photon escape efficiency, i.e., the probability of escape from the LED for photons generated by electron–hole recombination at the p/n junction. A major loss mechanism is due to the substrate, itself. When the substrate has a smaller bandgap than the photon energy, all photons propagating toward the substrate are absorbed. As an example, this is a major loss mechanism for InGaP LEDs grown lattice matched to GaAs substrates. Due to its small bandgap energy, GaAs absorbs all visible photons. Since photon emission in the GaInP is isotropic, the use of a GaAs substrate guarantees that approximately half of the emitted photons will be absorbed. The actual fraction absorbed is even greater due to total internal reflection of many

photons as they attempt to exit the very high refractive index semiconductor [35, 71]. There are two ways to overcome this problem: 1. Grow on high-bandgap substrates that do not absorb the photons, which is often not practical due to the lattice parameter mismatch to such substrates, which results in the production of dislocations where non-radiative recombination occurs, and 2. Remove the growth substrate and wafer-bond the epitaxial layer structure to a transparent "substrate", typically GaP, for mechanical support [35]. The latter is the technique commonly used for InGaP LEDs. It results in very high efficiency red and yellow LEDs; however, the substrate removal and wafer-bonding steps add significantly to the cost of the finished LED.

The use of nanotechnology suggests a novel, alternative approach—namely the growth of quantum wires on a transparent substrate. Dislocations due to the lattice parameter mismatch do not propagate into the quantum wires, as discussed in Sect. 1. The strain is relieved elastically since the wires are able to relax in the two directions orthogonal to the growth axis. Thus, the LED structure can be grown directly on a high-bandgap substrate such as GaP. The use of nanowires for both LED and laser devices is an active research area that will be described in Sect. 4.1.

As mentioned above, the other factor leading to the absorption of photons is total internal reflection due to the large refractive index of III/V semiconductors. Only the photons with directions within a cone, having an angle given by Snell's Law, are able to escape from the semiconductor [71, Chap. 5]. Photons striking the surface at all other angles are reflected back into the semiconductor, where they can be absorbed by the LED structure, itself, or the substrate. Decades ago, device designers were able to increase the solid angle for photon escape simply by encapsulating the LED in a transparent, high index material such as silicone or plastic. The LED can also be shaped into structures, such as truncated pyramids, that increase the fraction of photons that can escape from the LED [36].

More recently, techniques based on nanotechnology have been developed to improve the probability of photon escape. Simply roughening the surface produces surface angles that allow more of the photons to escape total internal reflection [71, Chap. 9]. A more controlled approach is to produce a periodic arrangement of surface structures, a "photonic crystal", at the surface that prevents total internal reflection. For example, an array of GaN nano-pyramids produced by etching [28, 57] produces a significant increase in light extraction efficiency.

As seen in Fig. 4, the combination of increasing the internal efficiency, using quantum wells as the light-emitting region, and using various techniques to increase photon escape, has produced red and blue LEDs having amazingly high external efficiencies of 55% in the red and well-above 60% in the blue. Figure 6 shows the structure used for low threshold current density blue lasers. LED structures are very similar. It will be noted that the InGaN is grown on a transparent sapphire substrate. This results in a very high defect level in the active layers. However, the sapphire is transparent, so photons can escape without absorption in the substrate. Since sapphire is an insulator, the laser and LED structures have both the n- and p-contacts on the top surface. This necessitates the growth of a high-conductivity buried n-type layer between the sapphire and the p/n

junction to avoid a high series resistance which results in low overall power efficiencies and non-uniform photon generation across the p/n junction. Typically, the LED devices are mounted upside-down so that the light emerges through the sapphire substrate. In some devices, the sapphire substrate is removed and the LED structure is bonded to a mirror mounted on an inexpensive, absorbing substrate, such as Si [57]. In this case, the p-contact is produced on the top of the device and the n-contact on the substrate. For this structure, which closely resembles the structure for InGaP LEDs, all of the photons are emitted from the top of the device.

3 Materials Issues for LEDs

The only materials to be discussed in this chapter are the III/V semiconductor alloys shown in Figs. 2 and 3. As mentioned above, the solid lines connecting the points for the individual compounds represent random ternary alloys, where the bandgap energy and lattice constant are uniquely specified by the solid composition. The areas between lines represent quaternary alloys, where the bandgap energy and lattice constant are independent parameters, both specified by the two solid composition parameters. These alloys were considered to be random or ideal during the early development of our understanding of these materials. The zinc-blende and wurtzite crystal structures in which the III/V materials crystallize can be thought of as two interpenetrating sublattices, with the group III atoms on one sublattice and the group V atoms on the other. A random ternary alloy consists of random mixing on one of the sublattices. Thermodynamically, this corresponds to an ideal mixture. As our understanding has matured, we have come to realize that non-random mixing, described in terms of the microstructure and, indeed, the nanostructure, can have a major role in determining the properties of the solid, particularly the bandgap energy, for an alloy having a specific composition. Thus, the bandgap energy is not uniquely specified by the solid composition, so the lines shown in Figs. 2 and 3 must be specified as being for random alloys.

Essentially all of the materials and structures described in this chapter are grown by the OMVPE technique. Early LED and laser devices were fabricated in the GaAs/AlGaAs system using the LPE technique. Problems with the growth of the phosphide and nitride alloys containing Al [79] as well as the difficulty of using LPE for the large-scale, high-yield processes required for inexpensive device manufacture have prevented it from becoming an important production method. Early LEDs in the GaAsP/GaAs system were made by HVPE, however, the same problems with the growth of Al-containing phosphide and nitride alloys has limited the application of this technique for LED and laser structures [79], although this process is used for the production of thick, compound semiconductor (typically GaP or GaN) layers for either window layers (GaP) or pseudo-substrate materials (GaN). MBE growth is a much more important technique. As mentioned above, it was the first to demonstrate the formation and advantages of nano-structures, particularly quantum wells, especially for laser devices. However, it has

proven to be a more expensive and less flexible production technique than OMVPE, which now dominates the commercial production of both AlInGaP and AlInGaN for LED and laser applications. Thus, only the OMVPE technique will be described in what follows.

OMVPE is a cold-wall technique where the source molecules, organometallic group III precursors, such as trimethyl-Ga, -In, and -Al, TMGa, TMIn, and TMAl, respectively, are combined with either hydride or organometallic group V molecules. Examples of the group V precursors are the hydrides, AsH_3, PH_3, and NH_3, and organometallic precursors, tertiarybutylarsine (tBAs), tertiarybutylphospine (tBP), and dimethylhydrazine $(CH_3)_2H_2N_2$. The precursors are introduced into the gas stream flowing over the substrate either by metering them from high-pressure cylinders, in which they may be diluted in hydrogen (typical for the hydrides), or by bubbling hydrogen through temperature-controlled reservoirs (typical for the low vapor pressure organometallic precursors). The precursors are present at pressures less than their room temperature vapor pressures, so they do not condense on the room temperature reactor walls. The only hot part of the reactor is the susceptor, on which the substrates are placed. When the gasses reach the heated substrate, they decompose to produce the desired elements on the surface of the single-crystalline substrate. They diffuse rapidly on the surface, reaching low-energy sites, typically at step edges [83].

The growth temperature is chosen to be sufficiently high to pyrolyze the precursors and to allow adequate surface mobilities to allow the growth of a highly perfect, single-crystalline solid. Normally, very high temperatures are avoided to minimize the generation of defects (due to entropy considerations) and incorporation of undesirable background impurities. Also, the growth rate decreases at high temperature for these highly exothermic processes for thermodynamic reasons [83, Chap. 1].

The growth process is optimized with respect to the substrate temperature and orientation, the total flow rate of the group III precursors, which determines the growth rate, and the ratio of group V to group III elements introduced into the vapor stream, the so-called "V/III ratio". OMVPE is a growth process that occurs with a very high supersaturation. This means that the free energy of the solid semiconductor produced is very much lower than that of the precursors at the growth temperature [83, Chap. 2]. Thus, OMVPE is sometimes referred to as a "non-equilibrium" process. However, in fact, a near-equilibrium state is typically reached between the solid and the vapor adjacent to the substrate during growth [83, Chap. 2]. Thus, thermodynamics normally determines many of the aspects of the growth process, itself, and the properties of the resulting solid.

One advantage of OMVPE is the versatility: essentially all III/V compounds and ternary and quaternary alloys as well as low-dimensional structures can be produced. MBE and chemical beam epitaxy (CBE) offer similar versatility, but the large-scale of OMVPE and the need for UHV equipment for MBE and CBE gives significant economic advantages to OMVPE. Thus, it is virtually the only technique used for the commercial production of LEDs and lasers, as well as other devices such as high performance, multijunction solar cells.

Some results obtained by MBE are included in this Chapter. MBE is a process that also operates at very high supersaturation. In this case, the elements are introduced into the vapor, an ultra-high vacuum in this case, by simple evaporation. Thus, the pure elements reach the surface by ballistic transport, where they react to form the solid [94].

During OMVPE growth, thermodynamics can be used to understand the solid composition in terms of the composition of the vapor and the growth temperature. For alloys with mixing on the group III sublattice, such as AlInGaP and AlInGaN, grown at relatively low temperatures with an excess of the group V element in the vapor phase, the group III distribution coefficients are unity [83, Chap. 2]. This means that the ratios of the group III elements in the solid are the same as those in the input vapor. This is an extremely important factor that allows the growth of these alloys with good control of solid composition [83, Chap. 2]. Thus, the alloys we are interested in, with Al, Ga, and In mixed on the group III sublattice, can easily be grown across the entire compositional range by OMVPE, but not by other techniques such as LPE or HVPE [79]. This is the key factor that has led to the dominant position of OMVPE for the growth of LED materials. MBE is the other technique capable of producing these alloys with good control of solid composition [11].

At the high growth temperatures typically used for the OMVPE growth of GaN (>1000°C), the volatility of metallic In means that the In distribution coefficient is less than unity and decreases with increasing temperature [4, 56, 83, Chap. 2]. The distribution coefficients for mixing on the group V sublattice can also be predicted from thermodynamics and these distribution coefficients are often far from unity and dependent on the growth parameters [83, Chap. 2].

One other factor is vital for the determination of the composition of the solid, independent of the growth technique. The equilibrium composition of the solid is determined by minimization of the free energy of the system. Since the strain energy of an epitaxial layer can be large, when the lattice parameter of the thin epitaxial layer or island differs from that of the substrate, a strain energy term must be included in the free energy. This gives rise to the so-called "lattice pulling" effect. It was first observed in InGaP layers grown on GaAs substrates by LPE [77]. The equilibrium solid composition of the coherent InGaP epitaxial layer was found to differ from the composition of tall, thin, rod-shaped crystallites formed around the edges of the epitaxial layer. The composition of the epi-layer was always pulled toward that giving a lattice parameter match with the substrate, a value of approximately $x_{In} = 0.5$. As discussed below, this is an important factor in determination of the composition of low-dimensional structures.

For thin epitaxial layers having a different equilibrium lattice constant than the substrate this difference is accommodated elastically. However, as the thickness of the epitaxial layer increases, a point is reached where the system begins to generate dislocation at the epilayer/substrate interface [71, Chap. 7]. The dislocations take the form of a cross-hatched array contained entirely in the interface plane. However, these dislocations interact, resulting in the propagation of so-called "threading dislocations" into the epitaxial layer. Dislocations are generally harmful to device

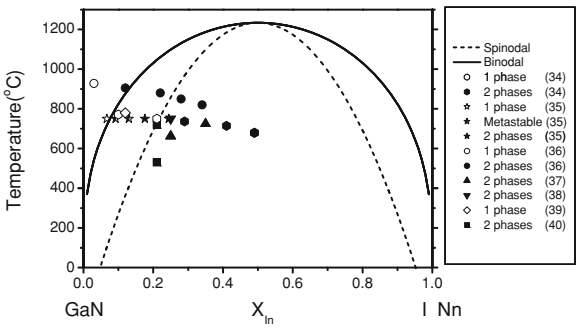

Fig. 8 Calculated bimodal (*solid*) and spinodal (*dashed*) curves [26] compared to experimental data [16, 18, 32, 63–65, 68] for InGaN. Open data points = single phase, half-filled data points = metastable, filled data points = 2 phase mixtures (after Stringfellow [85], with permission)

performance. They act as non-radiative recombination centers, and so reduce the internal quantum efficiency of LEDs, as shown in Fig. 7 and discussed in Sect. 1. They also result in an increase in the threshold current density of lasers. As described in Sect. 1, the exploration of methods for eliminating the misfit dislocations has been an important area of research, but no solutions have been discovered. Thus, the need for lattice matching, i.e., the selection of alloy composition to provide lattice matching with the substrate, has been a major constraint on the choice of materials to be used in LED structures. The use of quantum wires has recently emerged as a possible solution to this problem, as discussed in the next section.

The thermodynamics of semiconductor alloys was invoked above to describe the determination of solid composition and the effect of strain energy on the composition of strained epitaxial layers. An understanding of the thermodynamics of mixing of these alloys is also important for understanding the micro- or nano-structure produced spontaneously during growth. A number of models have been developed to understand the thermodynamics of III/V alloys. All of the models predict that the enthalpy of mixing is positive and is mainly determined by the size difference between the elements on the sublattice where mixing occurs [85]. The simplest model is the DLP model, where the enthalpy of mixing is proportional to the square of the difference in lattice constants between the two end components in a ternary alloy [78]. This correctly predicts that AlGaAs alloys are ideal solid solutions, i.e., the enthalpy of mixing (ΔH^M) is equal to 0, and that alloys, such as GaPN, where the lattice constants of GaP and GaN are very different, will have very large positive values of ΔH^M, leading to miscibility gaps [78]. The very important InGaN alloys are predicted to have a miscibility gap, as seen in Fig. 8 [26, 85]. This has enormous consequences for the micro- and nano-structures of these alloys [85].

Basic thermodynamics predicts that an AC–BC alloy with a positive enthalpy of mixing will spontaneously form clusters of like (AA or BB) atoms, while a negative enthalpy of mixing leads to ordering, where the number of AB pairs is larger than for a random alloy [88]. Thus, it was a surprise to discover that III/V alloys have a tendency to form *both* clusters and ordered structures. As described in detail below, clustering and PS are driven by the thermodynamics of the bulk for

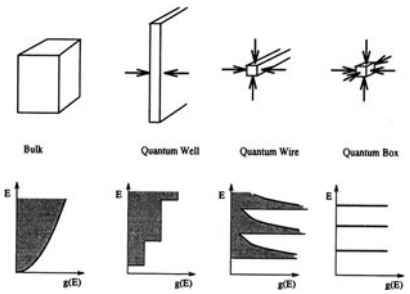

Fig. 9 Density of states, $g(E)$, as the number of confining dimensions is increased (after Adams and O'Reilly [2], with permission)

both InGaP and InGaN. However, when considering the surface thermodynamics, certain types of surface reconstruction lead to the formation of ordered structures, which may lead to significant reductions in the bandgap energy. Ordering is particularly important for the InGaP alloys used in red and yellow LEDs.

4 Natural and Artificial Nanostructures

Nanostructures will be defined here as structures with decreased dimensionality in either 1, 2, or all 3 directions, as shown in Fig. 8, with feature sizes of less than 30 nm. In the bulk, the zincblende or wurtzite structures are isotropic that is, the properties are independent of crystallographic direction and the wavefunctions for electrons (and holes) are Block functions, traveling waves in all 3 directions. The energy is nearly continuously variable. When the dimensionality is reduced in 1 direction (z), forming a 2D system, the wavefunctions in the x and y directions are still travelling waves. However, in the z direction, the wavefunctions are standing waves. This gives quantization of the energy in this direction. This is termed a quantum well when the well thickness is less than a de Broglie wavelength, approximately 30 nm. One may also count ordered structures as a part of this group of nanostructures since they consist of layered structures along specific crystallographic directions, forming a 2D system, although the periodicity is less than 1 nm. When the lattice periodicity is interrupted in two directions, the resulting structures are 1D quantum wires when the size of the structure is less than 30 nm.

When the lattice periodicity is interrupted in all 3 directions, forming a 0-D system, and the size is less than 30 nm, the structure is termed a QD. In this case, energy is quantized in all 3 directions. This gives a density of states for electrons like that of an atom, as shown in Fig. 9, consisting of discrete states, as discussed below. As the dimensionality of the system decreases the gain spectrum for lasing increases and becomes narrower [5], giving rise to a decrease in the threshold current density, J_{th}, as shown in Fig. 10. These nanostructures may form naturally during epitaxial growth. The spontaneous formation of both ordered structures and QDs will be discussed below. Additionally, quantum wells, wires, and dots can be

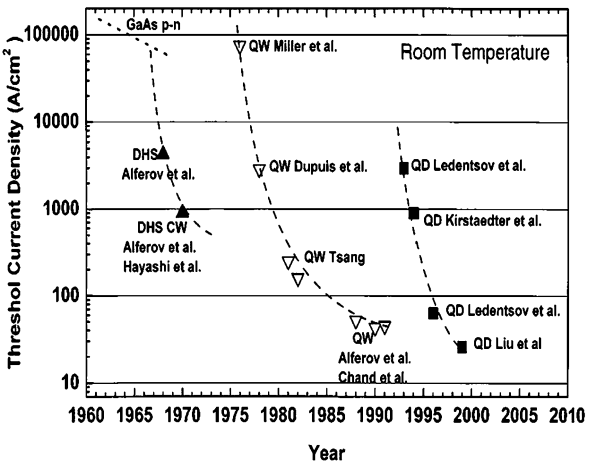

Fig. 10 Reduction of threshold current density from homojunction laser to double heterostructure, quantum-well, and quantum-dot lasers (reprinted with permission from Ledentsov et al. [44]. Copyright (2000), IEEE)

formed artificially, by switching the composition during growth, the use of masks, and other techniques. These will also be discussed in Sect. 4.1.

The first spontaneously-formed nanostructure to be discussed is atomic-scale ordering. In the 1980s, transmission electron microscopy (TEM) studies led to the surprising discovery that alloys such as AlGaAs, InGaP, and GaAsSb consisted of alternating monolayers (MLs) having different compositions along a particular crystallographic direction [82]. This was a phenomenon observed many years earlier in metal alloy systems; hence the nomenclature used refers to metallic systems: Cu-Pt (with ordering of {111} planes) and Cu-Au (with ordering of {100} planes). However, in metallic systems, the ordering process is driven by the thermodynamics of the bulk alloys. For systems with negative values of the ΔH^M, ordering is predicted to occur on the basis of simple thermodynamic calculations [83, 88, Chap. 2]. However, as discussed above, the enthalpy of mixing in semiconductor alloys is always greater than or equal to zero. Eventually, this apparent paradox was explained using surface thermodynamics. Real, low-index surfaces in semiconductor systems reconstruct [83, Chap. 3]. For growth by OMVPE where the V/III ratio is much greater than unity, the surface is typically terminated by group V atoms. The formation of dimer bonds between the group V atoms produces a (2×4) type of reconstruction composed of (110) dimer rows. The strain in the layers beneath these dimer rows provides a thermodynamic driving force for the formation of the Cu-Pt ordered structure [83, Chap. 3]. Thus, ordering is an example of a self-assembly process driven by surface thermodynamics.

Today, the degree of order has been firmly, empirically linked to the surface reconstruction [84]. An understanding of the thermodynamics and kinetics of growth has led to the ability to control the degree of order in epitaxial layers using parameters such as the growth temperature, V/III ratio, growth rate, and substrate misorientation [84]. Perhaps most interesting is the use of surfactants to control

ordering. It is found that elements such as Sb and Bi added to the system in small quantities during epitaxial growth act to suppress ordering. This is believed to be mainly due to the larger size of the surfactants that accumulate on the surface, which reduces the strain in the subsurface layers and, hence, the driving force for ordering [84].

For the InGaP system, ordering has major effects on the materials properties. For example, the bandgap energy can be reduced by 160 meV due to Cu-Pt ordering [87]. Of course, this has enormous consequences for LEDs. Those produced in disordered InGaP lattice matched to GaAs emit red light, whereas those produced in ordered material produce infrared radiation. Thus, ordering must be controlled. Similar considerations apply to the InGaP used in tandem solar cell applications, where, Sb is used to suppress ordering. In the important InGaN alloy system, ordering is much less prevalent and no one has yet demonstrated an effect on the bandgap energy.

Artificial structures similar to ordered structures are intentionally produced during epitaxial growth to produce superlattices and multiple quantum-well structures. For the production of the low-dimensional structures required for modern LED and laser devices, the growth technique must allow rapid changes in solid composition. The change in solid composition must occur over a distance of a single atomic layer for the growth of very thin quantum wells. MBE was the first technique to demonstrate such exquisitely fine control. However, extensive development efforts eventually allowed these fine structures to be controlled using OMVPE. Abrupt changes in solid composition require several factors: rapid gas switching, laminar flow (eddies provide for virtual memory effects), little or no memory due to adsorption/desorption on reactor walls, and atomically flat surfaces during growth [83, Chap. 9].

A novel type of quantum-well construction involves the growth of InGaN structures on patterned substrates. The In content and quantum-well thickness are dependent on the facet orientation [20, 21]. This gives the simultaneous emission of several different colors from a single epitaxial layer, which is potentially important for single-junction white LEDs.

Techniques similar to those described above were used in the initial attempts to produce quantum wire structures. In the GaAs/AlGaAs system, grown by MBE, Petroff et al. [62] produced quantum wire structures in the growth plane by using deposition at step edges on intentionally misoriented substrates. Selective growth techniques have also been used on patterned substrates to produce lateral quantum wires [31, 97]. Today, most quantum wire structures are produced in a vertical direction by using selective growth on the surface catalyzed by various techniques, including the addition of tiny Au balls to the surface (see, for example, Siefert et al. [74], Lauhon et al. [43], and Quian et al. [67]. In this case, the liquid Au catalyzes the low-temperature OMVPE growth, resulting in the production of a high density of nearly vertical wires each topped by a Au drop. The diameter of the wire is determined by the diameter of the Au droplets on the surface. Techniques have also been developed for the growth of nanowires without the use of Au droplets. As discussed below, quantum wires have properties that can be quite

different than the properties of thin epitaxial layers of the same solid composition, so are potentially interesting for both LED and laser devices.

The other nanostructure that yields desirable properties for light-emitting devices is the QD. Early research used masking techniques to produce 0D quantum structures [100, Chap. 6]. However, such techniques are unlikely to produce the desired results in an economical fashion. Thus, more recent research has focused on the self-assembly of collections of QDs. It is desirable to produce a high density of mono-dispersed QDs using rapid, simple growth techniques. The most promising technique is to take advantage of the Stranski–Krastanov (S–K) growth of strained epitaxial layers.

Strained epitaxial layers in semiconductor systems are normally found to grow by the S–K mechanism, involving the formation of a high density of small islands as well as a thin wetting layer [40, 96]. The S–K process for growth of a lattice-mismatched epitaxial layer produces a series of islands because the strain energy is lower than for a uniform layer; thus, there is a thermodynamic driving force for island formation [40, 73]. In S–K growth, a thin 1–2 ML uniform "wetting" layer is first formed by 2-D growth on the substrate. As growth continues, an array of three-dimensional (3D) islands forms spontaneously. The transition from 2-D to 3-D growth at a certain critical layer thickness has been observed for many semiconductor materials, grown by many techniques.

The phenomenon of S–K growth has been widely studied because the islands formed may constitute, when properly controlled, an array of QDs (QDs). This self-assembly process is a candidate as a practical technique for the fabrication of QDs for commercial injection laser devices, as discussed below. The reduced dimensionality of QDs gives rise to markedly superior device performance [45].

Among the first systems studied was the growth of Ge QDs on Si substrates. Strain-induced self-assembly of coherent islands was observed for Ge layers nominally a few MLs in thickness (see, for example, Ross et al. [70] and references therein). Of the III/V semiconductors, the growth of InAs and InGaAs QDs on GaAs has been perhaps the most widely studied. For example, Leonard et al. [46] found that $In_{0.5}Ga_{0.5}As$ coherently strained islands were spontaneously formed on (001) GaAs substrates by MBE after deposition of 4 ML of InGaAs. Moison et al. [53] studied the MBE deposition of InAs on GaAs. They found the transition from 2D to 3D growth to occur at a coverage of 1.75 ML. AFM measurements showed that islands 3 nm in height and 24 nm across were formed. The value of this self-assembly technique was shown by the remarkably uniform size of the islands formed. This is, of course, of vital importance for achieving the desired device performance. The OMVPE technique has been used to produce multi-layered QD structures in this system that have been used to produce injection laser devices with very low threshold current densities [45]. Interestingly, an early use of these InAs QD structures was to localize recombination in GaAs layers grown on Si substrates, where the high dislocation density kills the radiative recombination efficiency in homogeneous GaAs layers. When the density of the QDs exceeds the dislocation density, the InAs QDs collect the minority carriers for radiative recombination before they can reach a dislocation [23, 100].

4.1 Advantages of Nanotechnology

The major advantage of the use of low-dimensional structures with lengths of <30 nm was first recognized when quantum wells were found to allow GaAs, which has a bandgap energy giving IR photons, to emit visible photons [15]. This is based on the well-known quantum mechanical concept of a "particle in a box". For a 1-D box with a potential of 0 within the well and with infinite barriers, the energy levels of electrons are quantized

$$E_{\mathrm{n}} = \hbar^2/2m\,(n\pi/L_z)^2 \tag{4}$$

where L_z is the dimension of the 1D box, m is the effective mass, and n is the quantum number. This means that the lowest energy level of an electron in the conduction band of the well layer increases as L_z decreases. The same is true of the holes in the valence band. Thus, as the dimension L_z decreases the effective bandgap energy increases. This is termed the "quantum size effect" or QSE. For a finite well, the QSE is less than for the infinite well and the magnitude plateaus for very thin wells. Nevertheless, the QSE for electrons and holes results in photon energies considerably larger than the bandgap of the bulk materials. This adds an important degree of freedom to the design of the optimum material for an LED producing a specific wavelength of light. However, the advantages of low-dimensional nanostructures do not end here. By confining the electrons and holes to a small space, the wavefunction overlap increases, which leads to an increase in the matrix element for radiative recombination, in other words, the electrons and holes are squashed together which makes recombination to produce a photon more rapid. An additional advantage of low-dimensional structures for light-emitting devices is the increase in exciton binding energy [100]. This leads to exciton recombination at room temperature, which further significantly increases the rate of radiative recombination. The localization of recombination can also provide significant benefits in materials with high densities of dislocations and other defects by insuring that the electrons and holes are captured before they can reach the defects, where non-radiative recombination occurs. Thus, localization of recombination increases the radiative recombination rate and decreases the non-radiative recombination rate. Both effects lead to an increase in the internal quantum efficiency.

There is a potentially negative effect of electron and hole localization. The QCSE leads to a decrease in internal quantum efficiency for LEDs in (0001) quantum wells in the nitride systems. The nitrides crystallize in the hexagonal wurtzite structure, where strain in the (0001) direction gives rise to an electric field due to the piezoelectric effect. This field forces electrons and holes apart in the quantum well, leading to a reduction in the matrix element for radiative recombination [57]. However, this effect is diminished in very small QDs, where the electrons and holes are forced to occupy the same space in spite of the QCSE [54]. Thus, in addition to the benefits described above, the use of very small QD structures has the benefit of reducing the QCSE in the InGaN alloy system.

This offers the hope of a future improvement of green, yellow, and even red LEDs in this alloy system.

The use of coupled quantum wells opens the door to another type of laser, particularly suited to emission at very long wavelengths. In quantum-cascade lasers, the light-emitting transition occurs between the confined electron states in the quantum well [89, Chap. 12]. Thus, in this case, the photon energy can be much smaller than the bandgap energy. These lasers have been designed to operate at wavelengths as long as 70 μm.

The low-dimensional nanostructures produce a fundamental alteration of the band structure for semiconductor materials. In bulk material the density of states (number of states/unit of energy) increases as $E^{1/2}$ at the bottom of the band. For a quantum well, the density of states becomes independent of energy, with a much larger density of states at the bottom of the band. This leads directly to a decrease in threshold current density of lasers. Progressively more favorable density of states profiles in the conduction and valence bands are produced as the dimensionality of the nanostructures decreases, as shown in Fig. 9. This leads to increases in the gain at a given current density, and consequently progressive reductions in threshold current density for quantum wires and QDs, as seen in Fig. 10. The temperature dependence of the threshold current density is also dramatically improved as the dimensionality of the nanostructures decreases [100]. However, it is important to keep the volume of material where the emission actually occurs reasonably large. This requires a large number of QDs, often produced in several layers [45]. In addition, the size of the QDs, for example, must be uniform to avoid inhomogeneous broadening of the gain spectrum. Finally, to make the processes economically feasible, the QDs must be formed by a self-assembly process. This is normally accomplished by the production of the QDs by the S–K growth of strained materials.

Initially, quantum wires generated research interest due to the theoretically expected high electron mobilities [100, Sect. 26]. The geometry of wire structures provides the additional advantage for chemical and biological sensors of having a large surface area to volume ratio [59]. However, this may be a disadvantage for light-emitting devices, since surface recombination provides a non-radiative pathway. Thus, efficient LED operation may require use of core/shell nanostructures, where the high- bandgap shell prevents minority carriers in the core from reaching the surface.

Recent interest in quantum wires has centered on the use of vertical quantum wire structures as a self-assembly technique for the fabrication of tiny lasers [3]. This led to the unexpected discovery that the photoluminescence (PL) and LED efficiency of wires do not fall off as the amount of In in InGaN alloys increases. As mentioned above, and indicated in Fig. 4, for the MQW structures used for LED and laser devices, the radiative recombination efficiency falls dramatically as the In content increases above 15%. This extraordinary quantum wire behavior may partially be due to the much reduced dislocation density due to lattice mismatch in quantum wires, where lateral relaxation obviates the need for dislocation generation. However, this is unlikely to be the entire story. Compositional fluctuations

due to spinodal decomposition are more likely to occur in these unstrained structures, as discussed in Sect. 4.3, which may retard non-radiative recombination. Preliminary experimental results support this conclusion [27, 67]. Nevertheless, it is not entirely clear how PS is beneficial in structures having no dislocations. A third possibility is that PS occurs during growth (X. Niu et al., 2010, Controlled composition profiles of semiconductor alloy quantum dots and nanowires by selecting the growth mode, unpublished results) to spontaneously produce core/shell structures that retard surface recombination. A fourth possibility is that the removal of strain from the structure reduces the QCSE.

Nanostructured surfaces provide a further benefit for LEDs. They lead to less wave guiding in the high refractive index LED materials, resulting in an increased probability of photon escape. The nanostructured surfaces may consist of a periodic array of nano-sized features created on the surface by etching [57] or by selective-area, self-limiting growth. The roughened surface leads directly to an increase in the ratio of the number of photons escaping from the LED to the number produced at the p/n junction and, hence, the external quantum efficiency.

The use of low-dimensional nanostructures has become indispensable for LED and laser devices. It allows flexibility in the choice of the energy of the emitted photons, improves both the internal quantum efficiency and the photon extraction efficiency, and reduces costs by allowing the production of high-performance devices in highly defected materials, including those grown in lattice-mismatched to dissimilar substrates. The use of nanostructures, such as QDs and quantum wires, also offers promise for improvement of green, yellow, and even red LEDs in the InGaN alloy system.

The first system where the efficacy of nanostructures was demonstrated is the combination of GaAs and AlGaAs. Heterostructures in these materials yielded the first low threshold current density laser diodes and were intensively studied. One advantage of this materials system is that the lattice parameter is independent of the ratio of Al to Ga in the solid. Thus, high quality heterostructures can be grown epitaxially on GaAs substrates without the formation of misfit dislocations. As mentioned above, the bandgap of GaAs can be increased by sandwiching nm thick layers between layers of the higher bandgap AlGaAs. This was the beginning of "band gap engineering", the engineering of the properties of materials at the nanometer scale.

The need for lasers operating in the 1.3 and 1.55 μm wavelength ranges for long-distance, fiber-optic communication systems motivated early research. This application required bandgap energies lower than those of GaAs, leading to the development of GaInAsP, which can be grown lattice matched to InP substrates. In this materials system, a difficulty associated with limited solid miscibility was encountered that is associated with mixing elements having different covalent radii on the same sublattice, as discussed in Sect. 3. Miscibility gaps are more extensive in quaternary alloy systems, such as GaInAsP [83, Chap. 2]. Solid immiscibility led to difficulty in the growth of some alloys and adverse effects on materials properties, such as the electron mobility, where fluctuations in solid composition from spinodal decomposition produce scattering of free carriers [6].

Another system of interest is the simpler ternary GaInAs/GaAs system. However, the difference in covalent radii of Ga and In leads to misfit dislocations in thick layers with a significant In content grown on GaAs substrates. It was discovered that this problem can, again, potentially be overcome by the use of nanostructures. For very thin GaInAs layers grown on GaAs, the energy of strained GaInAs with no misfit dislocations is lower than that of GaInAs with misfit dislocations at the interface [50, 71, Chap. 7]. Thus, quantum-well structures can be fabricated with the desired 1.3 and 1.55 micron emission wavelengths. Interestingly, the strain inherent in such quantum-well structures gives a reduction in the hole effective mass, leading to reduced values of threshold current density [2]. It is, of course, vital to keep the well thickness below the critical layer thickness for dislocation generation. This system also became a vehicle for early investigations of even lower dimensional structures, such as quantum wires and QDs.

Since the beginnings of research on compound semiconductors, there has been a desire to grow epitaxial layers of these materials on Si substrates because Si substrates are much less expensive than GaAs or InP substrates and the integrated circuit business is based on Si. This is the third item of the overarching concerns articulated in Sect. 1. As an example, lasers grown on Si could be used for interchip communications, a current area of intensive research. There are a number of problems associated with GaAs growth on Si, but a major difficulty is with the generation of misfit dislocations due to the lattice parameter mismatch. The use of InGaAs QDs presents an ingenious solution to this problem. A high density of GaInAs QDs on a GaAs underlayer, generated by self-assembly of S–K islands, can mitigate the effects of dislocations in the GaAs generated by the lattice mismatch with the Si substrate [23, 99]. The minority carriers injected into the GaAs layer are captured by the smaller bandgap InGaAs regions before they can reach the dislocations where they generate the longer wavelength photons characteristic of the InGaAs, modified, of course, by the quantum size effect.

InGaAs/GaAs QD lasers have very low threshold current densities. The performance of lasers with QDs formed by the S–K process [45] have the lowest values of J_{th} reported due to the narrow gain spectrum, discussed in Sect. 2. However, the performance is still not optimal due to the dispersion in size of the self-assembled InGaAs QDs, giving rise to inhomogeneous broadening of the gain spectrum. Recent work has used the growth of QDs on the tops of pyramids formed using selective-area growth [102] to improve the control of QD size; however, this is necessarily an expensive process.

4.2 Importance of Nanostructures for AlInGaP Alloys

Early materials systems used for visible LEDs suffered from the presence of dislocations running through the p/n junction due to the lattice parameter mismatch with the substrate. For example, GaAsP was grown on GaAs substrates for early LEDs [14, 81]. The dislocation density could not be reduced below

approximately 10^6 cm^{-2}, even through the use of grading techniques to minimize dislocations at the GaAs/GaAsP interface [86]. As indicated in Fig. 7, this results in low quantum efficiencies of the order of 10^{-3} [81]. This is shown as the data point at the year 1968 on the plot of external quantum efficiency vs time in Fig. 5. The need for lattice-matched structures led to the development of $Ga_{0.5}In_{0.5}P$ grown on GaAs substrates [12, 14, 35, 81]. It was realized that the bandgap of this lattice matched structure could be increased by substituting Al for part of the Ga, forming the AlInGaP quaternary. In this system, the bandgap can be increased until, at high Al concentrations, the bandgap becomes indirect. As discussed above, indirect materials are very poor for light-emitting devices.

The push into AlInGaP alloys was a defining time in the development of materials for LEDs, since this alloy can only be grown by "non-equilibrium" techniques such as OMVPE [79] or MBE [11]. As discussed above, the high Al distribution coefficient makes growth by LPE or HVPE, the techniques used for AlGaAs and GaAsP, virtually impossible. This led to the domination of the LED industry by the OMVPE technique.

The development of OMVPE for the growth of AlInGaP for LEDs and lasers involved overcoming obstacles with unintentional incorporation of oxygen, which is known to kill the internal quantum efficiency [83, Chap. 8]. This is particularly problematic for alloys with high Al concentrations, since Al has such a high affinity for oxygen. P-type doping is also a problem, especially for the highest bandgap materials. In addition, ordering must be avoided in order to obtain the highest bandgaps. It is harmful to LED performance in this materials system. However, another nanostructure, namely QDs, is potentially beneficial, since QDs can have large direct bandgaps. This might be potentially useful for pushing the AlInGaP alloys to higher photon energies, beyond the direct–indirect transition for bulk alloys. Of course, the situation is complicated by the need for higher bandgap barrier materials.

4.2.1 Spontaneous Ordering

Early in the development of semiconductors for LED and laser applications, the materials properties of an alloy were considered to be uniquely specified by the solid composition. Over the last two decades a number of critically important micro- and nano-structural details, with dramatic impact on materials properties, have emerged for III/V alloys, including both AlInGaP and AlInGaN. Perhaps the simplest to analyze is atomic-scale ordering. The occurrence of ordering was unanticipated, since, as discussed in Sect. 3, the enthalpy of mixing for III/V alloys is always greater than or equal to zero: it is proportional to the difference in lattice constant squared [78]. Thus, for the widely studied InGaP alloys, used for red and yellow LEDs, the cation distribution is expected to be non-random; clustering and PS are predicted. Surprisingly, the opposite—atomic-scale ordering—is observed [83, Chap. 2, 84]. The basic thermodynamics of mixing predicts ordering only for alloys with a negative enthalpy of mixing [88]. For (001) InGaP alloys,

the ordering normally occurs in the form of a {111} ML superlattice, termed Cu-Pt ordering. This is a nanostructure with a periodicity of less than 1 nm. Formation of this structure is driven by surface thermodynamics [83, Chap. 3]. The driving force is the local, periodic strain associated with the surface reconstruction. Other ordered structures have also been observed, depending on the alloy system, the substrate orientation, the growth parameters, and the addition of surfactants during OMVPE growth [84, 87]. The order parameter has a major effect on the materials properties. Cu-Pt ordering is found to decrease the bandgap energy in $Ga_{0.5}In_{0.5}P$ by as much as 160 meV [87]. Thus, control of Cu-Pt ordering is important for LED and laser applications [84]. The use of ordering in InGaP with higher Ga concentrations has recently been suggested as a means of pushing the emission energies deeper into the green region of the spectrum [7]. It might similarly be used for AlInGaP alloys. Unlike the InGaP alloys, ordering does not appear to be a major factor determining the properties, in particular the bandgap energy, of InGaN, although it may adversely affect LED performance [54].

4.2.2 Artificial Nanostructures

Quantum wells are used in all high-performance AlInGaP LEDs and lasers. The use of quantum wells allows the production of high photon energies, in the orange and yellow regions of the spectrum, in materials with low Al concentrations, due to the QSE. This avoids the problems encountered at high Al concentrations, discussed above. In addition, quantum wells increase the radiative recombination rate.

Structures with lower dimensionality are also being explored in this materials system. As an example, small InP QDs dispersed in an AlInGaP matrix can be made to emit visible light [17] due to the QSE, even though InP has a smaller bandgap energy than GaAs, as seen in Fig. 2. The large band offsets in this system allow room temperature operation of lasers in the red region of the spectrum for data storage and medical applications. Room temperature InP QD lasers emitting at 740 nm have been reported [39]. They are also being considered for single photon sources for quantum cryptography emitting in the red, near the maximum sensitivity of Si photodetectors [72].

Quantum wire structures have also been fabricated using OMVPE with GaAs cores and InGaP shells [75]. The GaAs cores were grown using the standard vapor/liquid/solid (VLS) process at a low temperature of 450°C and the InGaP shells at higher temperature where growth can occur directly on the sides of the wires. The higher bandgap cladding layer inhibits surface recombination and so increases the GaAs PL intensity by a factor of 100–1000. The elastic strain from the cladding layer, when the Ga/In ratio is greater than unity, can be used to blue shift the emission from the core by as much as 240 meV. Thus, the quantum wire structures represent a method of tuning the emission wavelength. A similar increase in PL intensity was reported for GaAsP/GaP core–shell nanowires [52]. Significantly, in this case the spontaneous formation of a P-rich core was reported for GaAsP

nanowires grown by the VLS mechanism. This presents a potentially useful opportunity for the self-assembly of core–shell nanowires ((X. Niu et al., 2010, Controlled composition profiles of semiconductor alloy quantum dots and nanowires by selecting the growth mode, unpublished results)).

The use of nanostructured surfaces has been explored to increase the photon escape efficiency of AlInGaP LEDs. However, the effect is nearly eliminated when the LED chip is encapsulated in the polymer packaging material [71, p. 154].

4.3 Importance of Nanostructures for AlInGaN Alloys

InGaN and AlInGaN alloys have assumed increasing importance during the last decade. This is because the bandgap of AlInGaN can be tuned over the entire near IR to deep UV range, from 0.7 (bandgap of InN) to 6.2 eV (bandgap of AlN), as seen in Fig. 3. These alloys are essential for the commercial fabrication of blue, green, and white LEDs [4, 56]. However, the performance of yellow and, especially, red LEDs in this system is poor, solely because of a degradation of material quality at high In concentrations. These materials are also used for detectors, high power FETs and solar cells.

The AlInGaN alloys have proven to be most difficult to understand and control. The basic properties of the alloys are often masked by the large defect density induced by the lack of a native substrate. This typically means that they are grown on sapphire (or SiC) substrates having a dissimilar crystal structure, lattice spacing, and thermal expansion coefficient [4, 56]. This results in epitaxial AlInGaN layers having very high dislocation densities of 10^8–10^{10} cm^{-2}, in addition to stacking faults, twins, and other defects near the sapphire–epilayer interface [1]. GaN and InGaN alloys for device applications have been grown by MBE and HVPE techniques, but are nearly always grown by OMVPE for commercial LEDs and lasers. Typically, a thin GaN or AlN buffer layer is grown first at a low temperature followed by the high temperature (>1000°C) growth of a thick GaN or AlGaN layer. Then the InGaN is grown at a lower temperature, ranging from 700 to 900°C [55]. Typical LED structures consist of multiple quantum wells with well thicknesses of 2–3 nm and In contents ranging from 15% (blue) to 20% (green) InN, and even higher for yellow and red LEDs. The performance of these LEDs is stunningly good, considering the high density of threading dislocations. As discussed above (and shown in Fig. 7), in other III/V semiconductor materials systems a dislocation density of 10^8 cm^{-2} would be sufficient to kill the radiative recombination efficiency.

For LED performance, a number of materials issues turn out to be of critical importance. Issues relating to OMVPE growth, defect generation, and p-type doping, all major materials issues, will not be dealt with here. Instead, this section will concentrate on issues related to nanostructures in AlInGaN, or more frequently InGaN alloys.

The first issue to be considered is the control of alloy composition. In common with all III/V alloys, before the complexities of the micro- and nanostructures of

real AlInGaN alloys were fully appreciated, the sole parameter thought to control materials properties was the alloy composition. Thus, the bandgap energies of the ternaries included in the AlInGaN system are represented as solid lines in Fig. 3. The actual color of an LED with an InGaN active layer is, in fact, a function of the nominal alloy composition, but with additional effects from strain and the nanostructure.

For InGaP alloys, ordering is the most important naturally occurring nanostructure. For the InGaN alloys, a much more critical nanostructural phenomenon is the spontaneous formation of non-uniform alloys due to the occurrence of PS during growth. PS will be defined here as the occurrence of a non-uniform alloy composition on a nanometer scale. PS can be caused by a number of different effects. Even though random alloys have some degree of inhomogeneity, they are, by definition, a single phase.

First, we will consider the basic thermodynamics of InGaN alloys. Early valence force field calculations of Ho and Stringfellow [26] indicated that the phase diagram for bulk, unstrained, zincblende InGaN has a large region of solid immiscibility at typical InGaN growth temperatures. In Fig. 8, the region within the solid, binodal line defines the alloys that are thermodynamically unstable. Between the binodes the broken line indicates the spinode. For alloys having compositions between the spinodes at a given temperature, there is no energy barrier to PS, i.e., the solid is unstable to any compositional fluctuations. The calculated phase diagram gives a solubility of InN in GaN at 750°C of <5%. Later, more detailed first principles calculations have indicated that the equilibrium solubility may be even smaller, perhaps as small as 2% [22]. Even allowing for uncertainties in the calculations, the alloys used for blue and green MQW LEDs ($x = 0.15$ and $x = 0.20$, respectively) are well within the calculated region of solid immiscibility.

At equilibrium, these alloys could not be grown. In fact, the non-equilibrium growth of immiscible III/V alloys by OMVPE has been shown to be possible for many alloys [83, Chap. 2]. For thick InGaN epilayers, the beginnings of PS by spinodal decomposition occur during OMVPE growth for alloys within the miscibility gap as seen in Fig. 8. This gives rise to experimentally observed compositional fluctuations within the epitaxial layer. As seen in Fig. 8, the experimental data are in general agreement with the calculated phase diagram. Uniform layers were observed for In concentrations of less than the solid solubility (binode). For compositions between the spinode and the binode, the alloys are metastable. In these regions, an energy barrier must be surmounted for PS to occur. This suggests that PS may occur only near lattice disruptions, such as dislocations and other imperfections. Ponce et al. [64] reported that In-rich regions were formed only at elastically distorted regions of the layers, namely at dislocations, for these metastable alloys. As seen in Fig. 8, PS in this region is found to vary between the various experimental investigations. With larger In concentrations, giving alloys between the spinodes, spontaneous PS was observed throughout the layer in all experimental studies, as indicated in Fig. 8.

Analysis of the thermodynamics of alloy formation for InGaN in the elaborate structures used for MQW LEDs and lasers is more complex than the calculations

of [26], which are for incoherent, bulk systems. First, the strain energy associated with coherent spinodal decomposition (the formation of In-rich regions that are coherent, i.e., having no mismatch dislocations at the interfaces where x changes) will suppress PS. This is because coherent In-rich regions are under significant compressive strain in a more Ga-rich matrix, which has a high energy cost for the system. This coherency strain is predicted to completely suppress spinodal decomposition in most III/V alloys [80]. Second, biaxial strain due to lattice parameter mismatch between the substrate and underlying layers on the InGaN layer under consideration also significantly affects spinodal decomposition. InGaN coherently grown on GaN is under compressive strain. This mismatch strain, itself, suppresses the formation of In-rich clusters, since they have a larger equilibrium lattice constant than the matrix. Karpov [33] calculated the InGaN phase diagram, taking this strain energy into account. The results indicate that for $In_xGa_{1-x}N$, with $x = 0.15$ or 0.2, grown coherently on GaN, spinodal decomposition will be suppressed for typical growth temperatures.

Any understanding of these phenomena, as applied to the real InGaN materials used in the quantum wells of LED and laser devices, requires analysis of the mechanisms of epitaxial growth at the microscopic level. For example, strained epitaxial layers in semiconductor systems are normally found to grow by the S–K mechanism, described above, involving the formation of a high density of nanometer-sized islands as well as a thin wetting layer [40, 96]. This mechanism is expected to dominate the growth process for the InGaN quantum-well structures used in blue and green LEDs, due to the large lattice parameter mismatch with GaN. Thus, the good agreement between the experimental results and the phase diagram, as shown in Fig. 8, is perhaps surprising. Especially interesting are the results of Potin et al. [65] and Tran et al. [93] for QW structures.

S–K growth is expected for InGaN grown on GaN due to the large lattice mismatch of 11% between InN and GaN. A 2D to 3D transition is experimentally found to occur after a critical thickness of approximately three MLs [24]. Moustakis et al. [54] reported S–K growth of InGaN QDs on AlN by rf plasma assisted MBE. A transition from 2D to 3D growth occurred after the deposition of several MLs of InGaN. After 12 ML coverage, the average diameter and height of the InGaN islands, with $x = 0.43$, were 30 nm and 3 nm, respectively. Yamaguchi et al. [101] reported the S–K growth of InGaN islands on GaN by both MBE and OMVPE. RHEED studies during MBE clearly showed a 2D to 3D transition as the InGaN layer thickness increased. For samples grown by OMVPE, the 2D to 3D transition occurred for layer thicknesses of 4–5 nm, with an In concentration of 0.22. The aspect ratio for the faceted, entirely coherent islands was found to be approximately 2. Pristovsek et al. [66] used in situ ellipsometry to study the thickness at the 2D–3D transition in InGaN layers grown by OMVPE as a function of the In composition. They found a value of approximately 1.5 nm for $x_{In} = 0.20$ and a value of approximately 2 nm for $x_{In} = 0.15$. InGaN QDs 1–2 nm in height and 40–50 nm in diameter have been observed to form by the S–K growth mode during OMVPE growth by Jung et al. [30]. Self-assembled InGaN QDs were also produced by atmospheric pressure OMVPE by Tachibana et al. [90].

S–K growth was specifically demonstrated to occur for InGaN layers in MQW structures grown by OMVPE. In single quantum-well structures used for LEDs, Florescu et al. [19] reported, for the 3 nm wells containing approximately 15% InN, 3D, i.e., S–K, growth, giving much enhanced 300 K PL intensities. The effects of an inhomogeneous distribution of In on optical properties and device performance will be discussed below.

Efforts have been made to control spinodal decomposition during quantum-well growth, since it may be an important factor affecting device performance. One approach has been the use of anti-surfactants (Si in particular) in an effort to enhance QD formation during the S–K growth of InGaN on AlGaN by OMVPE. For growth at 800°C, Hirayama et al. [25] produced InGaN QDs in an AlGaN matrix for layers 3 nm thick. The diameter and height of the QDs were reported to be 10 and 5 nm, respectively. Intense room temperature PL was reported. Other authors have inserted buried layers to control the strain in the InGaN quantum-well layer(s). This will affect both the mismatch strain in the quantum-well layer(s) and the In incorporation, via the lattice pulling effect. Both will affect the formation of S–K islands. For example, Huang et al. [29] found enhanced emission efficiency for green InGaN/GaN QW LEDs when a prestrained buried layer was added. Park et al. [60] used surface roughening to enhance PS in thin InGaN layers grown on GaN. The layer thicknesses were less than the critical thickness for strain relaxation, t_c. However, intentional surface roughening was believed to produce unstrained, incoherent S–K islands. In the layers with enhanced spinodal decomposition, they observed intense PL emission from the In-rich regions at significantly lower energies than the PL of the material grown on flat GaN layers.

Lai et al. [42] used a five period InGaN/GaN MQW structure, grown by OMVPE at 780–880°C, with 2 nm InGaN wells, sandwiched by GaN to produce materials emitting at wavelengths from blue into the yellow region of the spectrum. They reported PS to occur due to spinodal decomposition during S–K growth of the InGaN, resulting in the formation of In-rich clusters, coherent with the matrix, having very uniform diameters. As discussed below, the control of PS to produce yellow emission is important for the fabrication of single junction, white LEDs.

In terms of the basic thermodynamics, discussed in Sect. 3, several phenomena can be expected to lead to PS for the S–K growth of *thin*, coherent InGaN islands on GaN. First, strain will suppress spinodal decomposition in coherent thin layers, but this constraint will be relaxed non-uniformly in S–K islands. In addition, the elastic relaxation will give more In incorporation in the more strain relaxed parts of the islands, due to the lattice pulling effect. Both phenomena will result in PS, i.e., the formation of local In-rich regions during growth [85].

The experimental evidence for the occurrence of PS in thin layers has been reviewed recently [85] and is overwhelming. EXAFS studies show the formation of non-random In distributions, characteristic of In clustering. Careful, high resolution TEM clearly shows a very high density of 2–4 nm In-rich regions. The CL and PL splitting as well as the Stokes shift are consistent with the formation of In-rich regions in a more Ga-rich matrix.

The spontaneous formation of QD structures during growth due to PS is of more than academic interest. Formation of In-rich clusters is found to have profound effects on the performance of laser and LED devices. PS will produce an emission wavelength in an LED or laser that is longer than expected for a random alloy because carriers collect in low-bandgap regions, so the emission energy is controlled by the local In composition. In addition, there is a great deal of evidence that the formation of In-rich nano-clusters produces a remarkable increase in radiative recombination efficiency in these highly dislocated materials. Chichibu et al. [13] were the first to explain this mystery in terms of localization of recombination at the In-rich clusters. Essentially, minority carriers are collected in the small bandgap regions at the In-rich clusters before they can recombine at dislocations. This yields an enormous increase in radiative recombination efficiency if the distance between the In-rich regions is smaller than the dislocation spacing. The S–K island density has been measured to be from 10^{10} to 10^{12} cm^{-2}, depending on growth conditions, which is orders of magnitude higher than the dislocation density in the high quality material used for high efficiency LEDs. Amazingly high values of external efficiency, well exceeding 60%, as seen in Fig. 4, have been reported for blue MQW LEDs in materials with extremely high dislocation densities, exceeding 10^{7} cm^{-2}. A dramatic increase in the external quantum efficiency as In is added to GaN in MQW LEDs, which increases the wavelength, is seen in Fig. 4. A small concentration of In gives a dramatic boost in LED efficiency. Indeed, it is impossible to produce high efficiency LEDs without the addition of In. The onset of this beneficial effect appears to coincide roughly with the onset of PS.

A major effect that may be related to the reduced radiative recombination in MQW LED structures with high In content is the QCSE. Wurtzite AlInGaN alloys are piezoelectric. Thus, stress along the c-axis of InGaN in quantum wells will give rise to a piezoelectric field that decreases the overlap between electron and hole wavefunctions. This results in a decrease in the quantum efficiency for the production of visible photons. As the In concentration increases, this QCSE increases. Thus, the efficiency of green LEDs would be expected to be lower than for blue LEDs. This is consistent with the well-known "green gap" discussed above. At the higher In concentrations required for yellow and red LEDs, the effect is even larger because of the increased piezoelectric field. This may, in part, explain their very low efficiencies. A beneficial effect of the QDs formed by PS may be that the deleterious effect of the QCSE is reduced by the formation of very small QDs, 1–2 nm in size. Of course, the wave function overlap will increase as the size of the QD decreases because the electrons and holes are squeezed together. This presents a promising approach for the development of longer wavelength InGaN LEDs. Moustakis and co-workers used MBE to produce small QDs that were used for green LEDs [1, 54]. This mechanism may also explain the improved yellow emission intensity obtained by Lai et al. [42] for InGaN grown by OMVPE, which is found to spinodally decompose to produce small-sized clusters behaving as quasi-QDs. Park et al. [61] used the S–K process for the self-assembly of InGaN QDs to produce a five layer LED structure. They specifically reported improved LED performance as the size of the QDs was decreased.

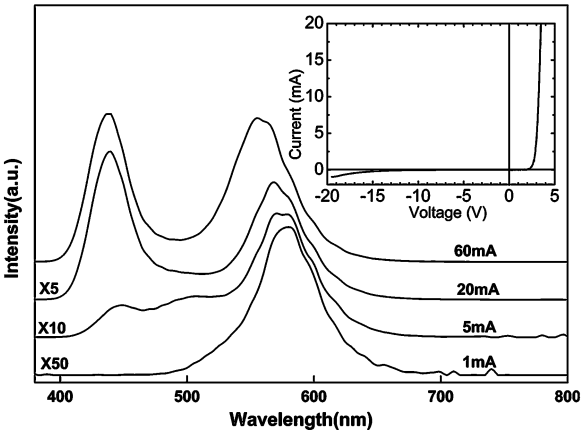

Fig. 11 Electroleuminescence spectra of InGaN layers with In-rich clusters at several currents (reprinted with permission from Wang et al. [98]. Copyright (2007), American Institute of Physics)

Recently, several strategies have been developed for the use of PS in InGaN for the production of white LEDs. The basic idea is to generate yellow photons in the InN-rich regions and blue photons in the matrix. Together, the light produced will appear as white. This is a very promising approach for white LEDs because the two competing techniques use either a blue LED and an overlayer of phosphor to down-convert some blue photons to yellow or the use of three (red, green, and blue) or sometimes four (adding yellow) individual LEDs packaged together. Both approaches have significant disadvantages. A white LED having a single p/n junction and no phosphor is very attractive.

Several approaches have been used to foster and control PS in the InGaN for white LEDs, as described above. Park et al. [60] used roughening of the surface to facilitate PS. The surface roughening is believed to produce incoherent In-rich InGaN islands. Other groups have used the control of strain in the epitaxial layers, using partially or completely relaxed buried layers, to control PS, as described above. These approaches are novel and promising. Wang et al. [98] used spinodal decomposition to form InN-rich QDs. The 220 nm thick underlying layer, containing 5% In, is relaxed, since the thickness is much greater than t_c. This is followed by a GaN layer and then the MQW structure. Four, 3 nm thick InGaN layers, containing 17% In form the well layers. Thus, the InGaN QW layers are partially relaxed, enhancing PS due to spinodal decomposition. The EL spectra reported by Wang et al. [98] are reproduced in Fig. 11. The yellow emission from the In-rich QDs and the blue emission from the more Ga-rich matrix are clearly resolved. The combined emission at high current densities looks white. These authors also demonstrated the production of In-rich regions using TEM. The results are reproduced in Fig. 12. InN rich QDs are clearly distinguished.

Lu et al. [48] also used an InGaN under-layer to reduce strain in the QW layers. They reported enhanced PS, as evidenced by TEM studies. Atomic level images

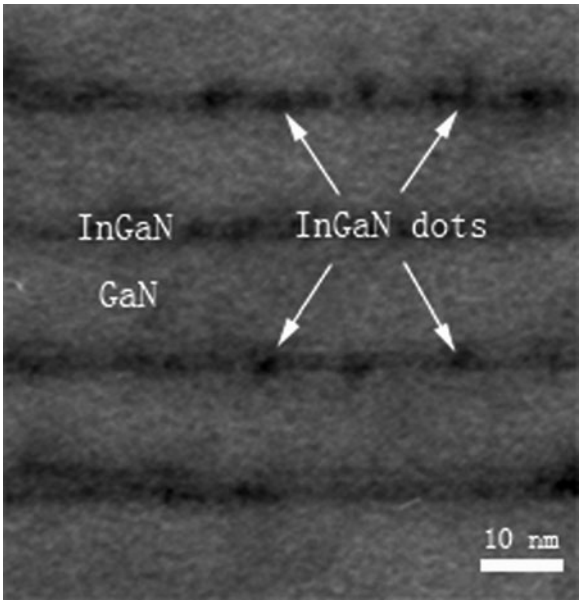

Fig. 12 Cross-section TEM image of the In-rich InGaN quantum dots in the LED structure giving the EL spectra shown in Fig. 11 (reprinted with permission from Wang et al. [98]. Copyright (2007), American Institute of Physics)

using strain state analysis yielded the In variation from QD to matrix in the light-emitting InGaN layers. They used changes in the thickness of the underlying, strain-relieving layer to produce values of the variation of In content from the In-rich region to the matrix of 14–18%, 15–25%, 17–37% and 18–49% as the pre-strained layer thickness was decreased. For five period MQW structures with 3 nm InGaN well layers, the best results were obtained with a 5 nm thick underlying layer having 7% In. This is less than the critical layer thickness, so the layers are coherent. Soh et al. [76] also made white LEDs using In-rich QDs to produce the yellow emission. They used dual stacked MQWs, using a complex procedure that includes the use of In as an antisurfactant.

Another approach to produce materials for improved green, yellow, and red LEDs in the AlInGaN alloys is the use of quantum wires. As mentioned above, the internal recombination efficiency of AlInGaN MQW structures drops dramatically as the In content of the InGaN is increased. There is evidence that quantum wires do not suffer from this behavior. Recent research [41] has shown that quantum wires grown by HVPE with bandgap energies across the entire visible spectrum emit PL with a near-constant efficiency. Work by Lieber and his group at Harvard has produced entire LED devices in triangular, core/multishell, radial InGaN nanostructures [67] that efficiently emit light from the purple through the yellow region of the spectrum (365–600 nm), with In concentrations of 1–35%. High quantum efficiencies of 5.8% at 440 nm and 3.9% at 540 nm were observed. They report the TEM observation of formation of localized In-rich clusters in the InGaN layers.

The reasons for the increased recombination efficiency in the longer wavelength InGaN wires have not been fully explained. One factor may be the absence of dislocations in the quantum wires, as described above**.** However, this does not appear to be the sole factor. Hong et al. [27] recently reported intense green PL from nanorod arrays grown by plasma assisted MBE. These authors report localized recombination in the quantum rods, with an increase in the localization depth as compared with 2D epitaxial layers. This is attributed to an increase in PS in the rods. This confirms the results of Quian et al. [67], discussed above. It is also consistent with the results for MQW samples that localization of the recombination is beneficial. The removal of elastic strain will increase the occurrence of spinodal decomposition, as described above. In this case the effect cannot be due to preventing minority carriers from reaching dislocations. Perhaps, the localization of recombination prevents recombination at other defects or at surfaces. This may tie in with the results described in Sect. 4.2.2 for GaAsP/GaP nanowires, where there was a natural segregation of the constituents in a lateral direction. This was confirmed for InGaN quantum wires grown by chemical vapor deposition using elemental sources and ammonia, where a natural segregation of Into the core of the wire was observed for Si substrates [10].

Another possible explanation is the decrease in the QCSE in rods, where the strain is relaxed elastically, thus removing the field due to the piezoelectric effect. Hong et al. [27] also report an increase in optical extraction efficiency for the samples made from quantum rods, as expected. A combination of these effects results in the PL intensity for the nanorod samples 15 times greater than that for InGaN layers with nearly the same composition.

5 Summary

The use of nanostructures, in the form of quantum wells, quantum wires, and QDs, has led to major advances in both the performance and affordability of visible LEDs, as summarized in Table 1. All commercial LED and laser devices across the entire spectrum from infrared to ultraviolet are fabricated using the OMVPE technique, using quantum wells to enhance performance. The quantum size effect leads to increased photon energies. This allows materials with bandgaps in the IR spectrum, such as GaAs and InP, to emit visible photons. In the commercially important AlInGaP and AlInGaN alloys, the use of quantum wells allows the desired color to be obtained while minimizing the amount of Al, a particularly difficult element due to C and O contamination, in the active region. The use of quantum wells also increases the radiative recombination rate and decreases the rate of non-radiative recombination. Both effects enhance the conversion efficiency of electrons into photons. The use of QDs yields even greater increases in LED performance as well as the lowest threshold current densities for laser devices. Current research is heavily directed to the use of QDs for increased performance of LEDs and lasers in the green, yellow, and red regions of the spectrum, as well as

Table 1 Advantages of nanostructures for light-emitting devices

Quantum wells	Increased bandgap energy as L_z decreases
	B_r increases as L_z decreases
	More favorable density of states for lasers and LEDs
Quantum wires	Increased free carrier mobility
	Increased bandgap energy as L_z, L_y decrease
	B_r increases as L_z, L_y decrease
	More favorable density of states for lasers and LEDs
	Relaxation of strain due to lattice mismatch, without dislocations
	Spontaneous phase separation during growth
Quantum dots	Increased bandgap energy as L_z, L_y, L_x decrease
	Stronger exciton binding energy
	B_r increases as L_z, L_y, L_x decrease
	Decrease in recombination at defect (including dislocation) sites
	Most favorable density of states (delta function) for lasers and LEDs
	Narrow electroluminescence and gain spectra
	Lowest threshold current densities for lasers
	No temperature dependence of threshold current density
	Reduced QCSE in InGaN
	Increased light extraction for photonic crystals on the surface

white LEDs, using AlInGaN alloys. The use of quantum wires also appears promising for such applications. Nanostructures on the surface have been demonstrated to increase the efficiency of extraction of photons generated within the LED. It is anticipated that future efforts to increase performance and decrease cost will center on the increased use of nanostructures.

References

1. Abell J, Moustakis TD (2008) The role of dislocations as nonradiative recombination centers in InGaN quantum wells. Appl Phys Lett 92:091901
2. Adams AR, O'Reilly EP (1996) Semiconductor band structure and related properties. In: Quillec M (ed) Materials for optoelectronics. Kluwer Academic, Boston, p 61
3. Agarwal R, Lieber CM (2006) Semiconductor nanowires: optics and optoelectronics. Appl Phys A 85:209
4. Akasaki I, Amano H (1997) OMVPE of GaN for high-brightness blue LEDs. In: Stringfellow GB, Craford MG (eds) High brightness LEDs. Academic Press, New York, Ch. 7
5. Asada M, Miyamoto Y, Suematsu Y (1996) Gain and threshold of three-dimensional quantum-box lasers. IEEE J Quantum Electron QE-22:1915
6. Benchimol JL, Quillec M, Slempkes S (1983) Improved mobility in InGaAsP alloys using high temperature LPE. J Cryst Growth 64:96
7. Bhusal L, Fluegel B, Steiner MA, Mascarenhas A (2009) Ordering induced direct–indirect transformation in unstrained GaInP for $0.76 < x < 0.78$. J Appl Phys 106:114909
8. Bjork MT et al (2002) One-dimensional heterostructures in semiconductor nanowhiskers. Appl Phys Lett 80:1058
9. Brown AS, Doolittle WA (2000) The status and promise of compliant substrate technology. Appl Surf Sci 166:392

10. Cai XM et al (2006) Straight and helical InGaN core-shell nanowires with a high In core content. Nanotechnology 17:2330
11. Casey HC, Panish MB (1978) Heterostructure lasers. Academic Press, New York
12. Chen CH, Stockman SA, Peansky MJ, Kuo CP (1997) OMVPE growth of AlGaInP for high-efficiency visible LEDs in high-brightness LEDs. In: Stringfellow GB, Craford MG (eds) High brightness LEDs. Academic Press, New York, Chap. 4
13. Chichibu S, Azuhata T, Sota T, Nakamura S (1996) Spontaneous emission of localized excitons in InGaN single and MQW structures. Appl Phys Lett 69:4188
14. Craford MG (1997) Overview of device issues in high-brightness LEDs. In: Stringfellow GB, Craford MG (eds) High brightness LEDs. Academic Press, New York, Chap. 2
15. Dingle R, Wiegmann W, Henry CH (1974) Quantum states of confined carriers in very thin $Al_xGa_{1-x}As$-GaAs-$Al_xGa_{1-x}As$ heterostructures. Phys Rev Lett 33:827
16. Doppalapudi D, Basu SN, Ludwig KF, Moustakas TD (1998) Phase separation and ordering in InGaN alloys grown by molecular beam epitaxy. J Appl Phys 84:1389
17. Eichfelder M et al (2009) Room-temperature lasing of electrically pumped red-emitting InP/AlGaInP quantum dots embedded in a vertical microcavity. Appl Phys Lett 95:131107
18. Faleev N et al (2009) Correlation of crystalline defects with photoluminescence of InGaN layers. Appl Phys Lett 95:051915
19. Florescu DI et al (2004) AFM and temperature-dependent photoluminescence studies of the degree of localization induced by quantum-dot like states in InGaN single quantum well light emitting diodes grown by MOCVD on (0 0 0 1) sapphire. J Cryst Growth 272:449
20. Funato M et al (2006) Tailored emission color synthesis using microfacet quantum wells consisting of nitride semiconductors without phosphors. Appl Phys Lett 88:261920
21. Funato M et al (2008) Emission color tunable LEDs composed of InGaN multifacet quantum wells. Appl Phys Lett 93:021126
22. Gan CK, Feng YP, Srolovitz DJ (2006) First-principles calculation of the thermodynamics of InGaN alloys. Phys Rev B 73:235214
23. Gerard JM, Cabrol O, Sermage B (1996) InAs quantum boxes: Highly efficient radiative traps for light emitting devices on Si. Appl Phys Lett 68:3123
24. Grandjean N, Ilegems M (2007) Visible InGaN/GaN quantum-dot materials and devices. Proc IEEE 95:1854
25. Hirayama H, Tanaka S, Ramvall P, Aoyagi Y (1998) Intense photoluminescence from self-assembling InGaN quantum dots artificially fabricated on AlGaN surfaces. Appl Phys Lett 72:1736
26. Ho IH, Stringfellow GB (1996) Solid phase immiscibility in GaInN. Appl Phys Lett 69:2701
27. Hong CC, Ahn H, Wu CY, Gwo S (2009) Strong green PL from InGaN/GaN nanorod arrays. Opt Express 17:17337
28. Huang HW et al (2006) Improvement of InGaN/GaN LED performance with a nono-roughened p-Gan surface by excimer laser-irradiation. Mater Chem Phys 99:414
29. Huang C et al (2008) Enhanced efficiency and reduced spectral shift of green LED epitaxial structure with prestrained growth. J Appl Phys 104:123106
30. Jung W, Jang J, Choi S, Kim J (2008) Growth behavior of InGaN/GaN quantum dots structure via MOCVD. Korean J Mater Res 18:535
31. Kapon E, Hwang DM, Bhat R (1989) Stimulated emission in semiconductor quantum wire heterostructures. Phys Rev Lett 63:430
32. Kar A, Alexson D, Dutta M, Stroscio MA (2008) Evidence of compositional inhomogeneity in $In_xGa_{1-x}N$ alloys using ultraviolet and visible Raman spectroscopy. J Appl Phys 104:073502
33. Karpov SYu (1998) Suppression of phase separation in InGaN due to elastic strain. MRS Internet J Nitride Semicond Res 3:16
34. Keiser G (1991) Optical fiber communications, 2nd edn. McGraw-Hill, Inc, New York, Chap. 4
35. Kish FA, Fletcher RM (1997) AlGaInP LEDs. In: Stringfellow GB, Craford MG (eds) High brightness LEDs. Academic Press, New York, Chap. 5

36. Krames M et al (1999) High-power truncated-inverted-pyramid AlGaInP/GaP LEDs exhibiting >50% external quantum efficiency. Appl Phys Lett 75:2365
37. Krames MR et al (2000) High brightness AlGaInN light emitting diodes. Proc SPIE 3938:2
38. Krames MR et al (2007) Status and future of high-power light-emitting diodes for solid-state lighting. J Display Technol 3:160
39. Krysa AB et al (2007) Low threshold InP/AlGaInP on GaAs QD laser emitting at 740 nm. J Cryst Growth 298:663
40. Kukta RV, Freund LB (1997) J Mech Phys Solids 45:1835
41. Kuykendall T, Ulrich P, Aloni S, Yang P (2007) Complete composition tunability of InGaN nanowires using a combinatorial approach. Nat Mater 6:951
42. Lai Y, Liu C, Chen Z (2006) Tuning the emitting wavelength of InGaN/GaN superlattices from blue, green to yellow by controlling the size of InGaN quasi-quantum dot. Thin Solid Films 498:128
43. Lauhon L, Gudiksen M, Wang D, Lieber CM (2002) Epitaxial core-shell and core-multishell nanowire heterostructures. Nature 420:57
44. Ledentsov NN et al (2000) Quantum-dot heterostructure lasers. IEEE J Sel Top Quantum Electron 6:439
45. Ledentsov NN, Bimberg D, Alferov ZhI (2008) Progress in epitaxial growth and performance of quantum dot and quantum wire lasers. J Lightwave Tech 26:1540
46. Leonard D et al (1993) Direct formation of quantum-sized dots from uniform coherent islands of InGaAs on GaAs surfaces. Appl Phys Lett 63:3203
47. Lester SD, Ponce FA, Craford MG, Steigerwald DA (1995) High dislocation densities in high efficiency GaN-based LEDs. Appl Phys Lett 66:1249
48. Lu C, Huang C, Chen Y, Yang CC (2008) Dependence of spectral behavior in an InGaN/GaN quantum-well light-emittingdiode on the prestrained barrier thickness. J Appl Phys 104:043108
49. Luo JW, Franceschetti A, Zunger A (2008) Quantum-size-induced electronic transitions in quantum dots: indirect band-gap GaAs. Phys Rev B 78:035306
50. Mathews JW, Blakesley AE (1976) Defects in epitaxial multilayers: III. Preparation of almost perfect multilayers. J Cryst Growth 32:265
51. Mishra U (2008) Group III nitride optoelectronics, Invited talk at electronic materials conference, Santa Barbara California
52. Mohseni PK et al (2009) Structural and optical analysis of GaAsP/GaP core-shell nanowires. J Appl Phys 106:124306
53. Moison JM et al (1994) Self-organized growth of regular nanometer-scale InAs dots on GaAs. Appl Phys Lett 64:196
54. Moustakis TD et al (2008) Growth of III-nitride QDs and their applications to blue-green LEDs. Phys Stat Sol (a) 205:2560
55. Mukai T (2002) Recent progress in group-III nitride LEDs. IEEE J Sel Top Quantum Electron 8:1077
56. Nakamura S (1997) Group III–V nitride-based ultraviolet blue–green–yellow LED and laser diodes. In: Stringfellow GB, Craford MG (eds) High brightness LEDs. Academic Press, New York, Chap. 8
57. Nakamura S (2009) Current status of GaN-based solid-state lighting. MRS Bull 34:101
58. Narukawa Y et al (2006) Ultra-high efficiency white LEDs. Jpn J Appl Phys 45:L1084
59. Novotny CJ, Yu ET, Yu PKL (2008) InP nanowire/polymer hybrid photodiode. Nano Lett 8:775
60. Park I et al (2005) Enhancement of phase separation in the InGaN layer for self-assembled In-rich quantum dots. Appl Phys Lett 87:061906
61. Park I et al (2008) Effect of InGaN quantum dot size on the recombination process in light-emitting diodes. Appl Phys Lett 92:253105
62. Petroff PM, Gossard AC, Wiegmann W (1984) Structure of AlAs-GaAs interfaces grown on (100) vicinal surfaces by molecular beam epitaxy. Appl Phys Lett 45:620

63. Piner EL, El-Mastry NA, Liu SX, Bedair SM (1998) Phase separation in InGaN grown by metalorganic chemical vapor deposition. Mater Res Soc Proc 482:125
64. Ponce FA et al (2003) Microstructure and electronic properties of InGaN alloys. Phys Stat Sol (b) 2:273
65. Potin V et al (2004) Comparison of the In distribution in InGaN/GaN quantum well structures grown by MBE and MOVPE. J Cryst Growth 262:145
66. Pristovsek M, Stellmach J, Leyer M, Kneissl M (2009) Phys Stat Sol C 6:5565
67. Quian F, Gradecak S, Li Y, Wen CY, Lieber CM (2005) Core/multishell nanowire heterostructures ad multicolor, high-Efficiency LEDs. Nano Lett 5:2287
68. Rao M, Kim D, Mahajan S (2004) Compositional dependence of phase separation in InGaN layers. Appl Phys Lett 85:1961
69. Reynard J, Kandaswarmy PK, Monroy E, Gayral B (2009) Suppression of nonradiative processes in long-lived polar GaN/AlN quantum dots. Appl Phys Lett 95:131903
70. Ross FM, Tersoff J, Tromp RM (1998) Coarsening of self-assembled Ge quantum dots on Si (001). Phys Rev Lett 80:984
71. Schubert EF (2006) Light-emitting diodes, 2nd edn. Cambridge Press, Cambridge
72. Schultz WM et al (2009) Optical and structural properties of InPquantum dots embedded in $(Al_xGa_{1-x})_{0.51}In_{0.49}P$. Phys Rev B 79:035329
73. Siefert W et al (1997) In situ growth of nanostructures by MOVPE. J Cryst Growth 170:39
74. Siefert W et al (2004) Growth of one dimensional nanostructures in MOVPE. J Cryst Growth 272:211
75. Skold N et al (2005) Growth and optical properties of strained GaAs-GaInP core-shell nanowires. Nano Lett 5:1943
76. Soh CB et al (2008) Cool white III-nitride LEDs based on phosphor-free indium-rich InGaN nanostructures. Appl Phys Lett 92:261909
77. Stringfellow GB (1972) The importance of lattice mismatch in the growth of GaInP epitaxial crystals. J Appl Phys 43:3455
78. Stringfellow GB (1974) Calculation of ternary and quaternary III–V phase diagrams. J Cryst Growth 27:21
79. Stringfellow GB (1978) VPE growth of III/V semiconductors. Annu Rev Mater Sci 8:73–98
80. Stringfellow GB (1982) Spinodal decomposition and clustering in III/V alloys. J Electron Mater 11:903
81. Stringfellow GB (1997) Materials issues in high-brightness LEDs. In: Stringfellow GB, Craford MG (eds) High brightness LEDs. Academic Press, New York, Chap. 1
82. Stringfellow GB (1998) Ordering in III/V semiconductor alloys. In: Santos M, Liu WK (eds) Thin films: heteroepitaxial systems. World Scientific Publishing, Hackensack, pp 64–116
83. Stringfellow GB (1999) Organometallic vapor phase epitaxy: theory and practice, 2nd edn. Academic Press, Boston
84. Stringfellow GB (2002) Effects of the surface on CuPt ordering during OMVPE growth. In: Mascarenhas A (ed) Spontaneous ordering in semiconductor alloys. Kluwer Academic Publishers, New York, Chap. 3
85. Stringfellow GB (2010) Microstructures produced during the epitaxial growth of InGaN alloys. J Cryst Growth 312:735
86. Stringfellow GB, Greene PE (1969) Dislocations in GaAsP. J Appl Phys 40:502
87. Su LC, Ho IH, Kobayashi N, Stringfellow GB (1994) Order/disorder heterostructures in GaInP with $\Delta E = 160$ meV. J Cryst Growth 145:140
88. Swalin RA (1972) Thermodynamics of solids. Wiley, New York
89. Sze SM, Ng KK (2007) Physics of semiconductor devices, 3rd edn. Wiley, New York
90. Tachibana K, Someya T, Arakawa A (1999) Nanometer-scale InGaN self-assembled quantum dots grown by metalorganic chemical vapor deposition. Appl Phys Lett 74:383
91. Takagahara T, Takeda K (1992) Theory of the quantum confinement effect on excitons in quantum dots of indirect-gap materials. Phys Rev B 46:15578

92. Tanoto H et al (2009) Electroluminescence and structural characteristics of InAs/InGaAs QDs grown on graded SiGe/Si substrate. Appl Phys Lett 95:141905
93. Tran CA et al (1998) Phase separation in InGaN/GaN MQWs and its relation to brightness of blue and green LEDs. J Cryst Growth 195:397
94. Tsao JY (1993) Materials fundamentals of molecular beam epitaxy. Academic Press, Boston
95. Vampola KJ et al (2008) Highly efficient broad-area blue and white LEDs on bulk GaN substrates. Phys Stat Sol (a) 206:200
96. Venables JA (2000) Introduction to surface and thin film processes. Cambridge University Press, Cambridge, pp 145–146
97. Wang XL, Ogura M, Matsuhata H (1995) Flow rate modulation epitaxy of AlGaAs/GaAs quantum wires on nonplanar substrate. Appl Phys Lett 66:1506
98. Wang XH et al (2007) White LEDs based on a single InGaN emission layer. Appl Phys Lett 91:161912
99. Weisbuch C, Nagle J (1990) Science and engineering of 1D and 0D semiconductor systems, ser. NATO ASI series. Plenum, New York, p 319
100. Weisbuch C, Vinter B (1991) Quantum semiconductor structures: fundamentals and applications. Academic Press, Boston
101. Yamaguchi T et al (2006) Two to three dimensional transitions of InGaN and the impact of GaN overgrowth. Phys Stat Sol (c) 3:1396
102. Yuan J, Wang H, van Veldhoven PJ, Notzel R (2009) Impact of base size and shape on formation control of multifaceted InP nanopyramids by selective area MOVPE. J Appl Phys 106:124304